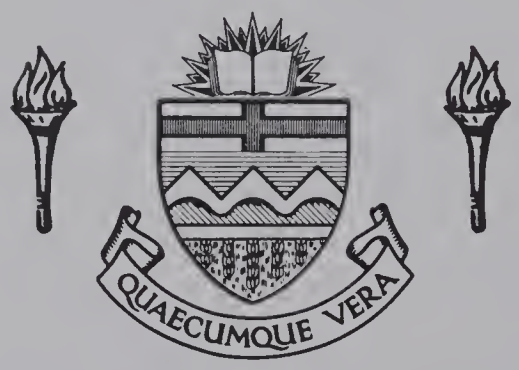

THE UNIVERSITY OF ALBERTA

STREAMLINE PATTERNS AND TERRAIN-INDUCED VERTICAL VELOCITIES IN THE CANADIAN CORDILLERA

BY

© CECILIEN O. CHARETTE

A THESIS

SUBMITTED TO THE FACULTY OF GRADUATE STUDIES AND RESEARCH

IN PARTIAL FULFILMENT OF THE REQUIREMENTS FOR THE DEGREE

OF MASTER OF SCIENCE

DEPARTMENT OF GEOGRAPHY

EDMONTON, ALBERTA

FALL, 1971

UNIVERSITY OF ALBERTA

FACULTY OF GRADUATE STUDIES AND RESEARCH

The undersigned certify that they have read, and recommend to the Faculty of Graduate Studies and Research for acceptance, a thesis entitled "Streamline Patterns and Terrain-induced Vertical Velocities in the Canadian Cordillera", submitted by Cecilien O. Charette in partial fulfilment of the requirements for the degree of Master of Science.

ABSTRACT

The complex problem of the low-level circulation in the Canadian Cordillera is explored in this study by examining the stream-line patterns of five synoptic situations at the 850-mb level. Each of the five patterns represents a typical flow regime of different orientation and orographic aspect.

A stream-function is used to describe the atmospheric flow. The function is first calculated at synoptic network radiosonde and pilot balloon stations, as well as at a number of interpolated auxiliary data points. The analysis is then extended by an objective method to the points of a one-quarter (95.25 km) mesh grid superimposed on the Western Cordillera. The orientation of the grid is such that its rows and columns run, respectively, normal and parallel to the major mountain ranges.

Quantitative estimates of terrain-induced vertical velocities are calculated for each case. For this purpose, the air is assumed to surmount every obstacle of a smoothed profile of the region covered by the grid. The equation used to calculate the vertical velocity w is

$$w = \vec{V} \cdot \nabla H \ ,$$

where $\vec{V}$ is the horizontal wind velocity and H is the height of the terrain. The orographic effects on the flow are assumed to decrease linearly to zero at a vertical distance of 3 km above the terrain.

The horizontal wind component $\vec{V}$ is computed from the gradient of the stream--function. Because the finite difference method used to approximate the above equation requires values at discrete grid points,

the height H at a given one-quarter grid point should be representative also of the surrounding area. Consequently, the heights of all the nearest-neighbor one-eighth-mesh grid points were found, and a representative mean height was calculated by giving a weight of 0.4 to the height at the central one-quarter point and a weight of 0.6 to the mean height of the eight nearest neighbors.

The results of the analysis are presented on two maps for each of the five synoptic cases. The first map displays the results of the objective analysis in unmodified form, including isotachs of vertical velocity at intervals of 2 cm/sec. Discontinuities develop in the computed streamline pattern where the high terrain pierces the 850-mb surface. The second map tentatively suggests the probable deflection of air streams around the more prominent peaks and ridges. On both maps the complexity of the low-level atmospheric flow in the mountainous regions is shown in new detail and, in particular, the major passages for air flowing into Alberta and the Yukon are indicated. Although some of the orographic vertical velocities appear too large, they are at least of relative importance in bringing out the significant ridges and obstacles which impede the atmospheric flow.

ACKNOWLEDGEMENTS

This thesis must be prefaced by a tribute to those many individuals who have cooperated in making it a reality.

I am indebted to my departmental supervisor, Dr. E. R. Reinelt, for his guidance, his valuable suggestions, and his thorough review of this report. I am pleased to thank Professor R. W. Longley for his help and comments, and also Dr. J. P. Penny for his readiness to serve on the examination committee.

I greatly appreciated the assistance of Mr. Y. S. Chung in gathering the data and in analyzing maps. The patience and outstanding competence of Mrs. Laura Smith who typed both the first and final drafts is gratefully acknowledged.

Without the facilities of the University of Alberta Department of Computing Science, the analysis of the data would have been impossible. I wish to express my appreciation to the technical staff of the Department of Geography for their splendid cooperation. Finally, I wish to thank also Mr. J. H. R. Noble, Assistant Deputy Minister, Atmospheric Environment Service (Department of Environment) for providing the financial support while on educational leave at the University of Alberta.

TABLE OF CONTENTS

LIST OF FIGURES

CHAPTER I

MOUNTAIN EFFECTS ON WEATHER

Introduction

Air flow across mountain barriers, terrain-induced vertical motions, and related effects such as orographic rain constitute difficult problems in meteorology. Numerous researchers are engaged in solving these problems, and dynamic meteorologists in particular are expending great effort trying to include orographic effects in ever more realistic numerical models of the atmospheric circulation.

Mountains and Weather

Bonacina (1945) used the following expression to describe the effects of mountains on the weather: "Mountains of all dimensions, high or low, the world over are in some measure storm breeders and the generators of all kinds of bad weather." The high ground obstructs the circulation and impedes the free flow of the wind which has, therefore, to surmount the obstacle or go around it. Almost any precipitation map shows a banded structure of isohyets paralleling the ridges of high ground.

Orographic Precipitation

During the last fifty years the problem of orographic rain has held the interest of many meteorologists in different parts of the world. J. Bjerknes and H. Solberg (1921) considered the effect of the Norwegian Mountains on the formation of rain. Similar studies were

conducted later by J. Douglas and J. Glasspoole (1947) and J. Sawyer (1952, 1956) in the British Isles. More recently, E. R. Reinelt (1969) has studied the role of orography in the precipitation regime of Alberta.

Numerical models, used to produce quantitative precipitation forecasts, such as developed by Harley (1965) and by Smagorinsky and Collins (1955), incorporate a component of vertical velocity induced by orographic barriers.

Elliott and Shaffer (1962) have summarized the importance of short-period quantitative forecasts in mountain areas. It is obvious that reliable forecasts could provide the basis for vital decisions in the management of flood control, water conservation facilities, and weather modifications.

Basic Principles of the Present Study

Although this particular study does not consider orographic precipitation, it could be a starting point towards this objective in western Canada. It takes a closer look at the large-scale synoptic flow crossing the Canadian Rockies. In addition, quantitative estimates of terrain-induced vertical velocities are computed. It is based on a similar study by Jarvis and Agnew (1970) for the Appalachian Mountains. The approach is simple and uses the stream-function to describe the flow. The winds to be used in the calculation of vertical velocities are obtained from the stream-function gradient. Since the stream-function is related to the geostrophic wind, an upper-air pressure level is considered instead of the friction layer near the earth's surface. Its choice is restricted by the amount of pertinent information which is normally more abundant in the lower levels of the atmosphere.

In the present case, the 850-mb pressure surface is a good choice. It is realized that the geostrophic flow is a rather crude assumption to make at this level, especially in mountain regions, but it is a worthwhile first measure of orographic flow conditions which should be considered before more sophisticated approaches are tried. The 850-mb flow is definitely influenced by the mountains and can in fact be used to calculate terrain-induced vertical velocities.

This study first describes the relationship that exists between a stream-function and a streamline, and then presents a complete description of the model used. The difficulties encountered and the attempts to overcome them are discussed before a treatment of five different synoptic situations is given. Conclusions and suggestions for further work are offered in the final chapter.

CHAPTER II

THE STREAM-FUNCTION - STREAMLINE RELATIONSHIP

Introduction

Streamlines are commonly used in fluid mechanics to represent the flow of a fluid. In meteorological applications streamlines are particularly useful for depicting flow patterns in the tropics where the circulation is weak and the Coriolis effect is small. If the divergence is zero, streamlines may be expressed conveniently in terms of a stream-function (see e.g. Tietjens, 1934, or Whitaker, 1968).

The Differential Streamline Equation

A streamline is defined as a curve which is tangential to the flow at a given instant. Thus, by definition, the fluid cannot cross a streamline but only flow along it (see Sutton, 1949, p. 35).

In general the condition of tangency may be expressed by

$$\vec{V} \times \vec{dr} = 0 , \qquad (2\text{-}1)$$

where $\vec{V}$ is the velocity and $\vec{dr}$ the line element of the streamline. Writing $\vec{V}$ and $\vec{dr}$ in component form, equation (2-1) becomes, for two-dimensional flow in the x - y plane

$$udy - vdx = 0, \qquad \text{or} \qquad \frac{dy}{dx} = \frac{v}{u} . \qquad (2\text{-}2)$$

This is the differential equation for a family of streamlines in two-dimensional horizontal flow (Petterssen, 1956).

The Stream-Function

The following derivation is based on the formal development of the stream-function by Whitaker (1968). The fluid is assumed to be incompressible and the motion is considered to be parallel to the x-y plane.

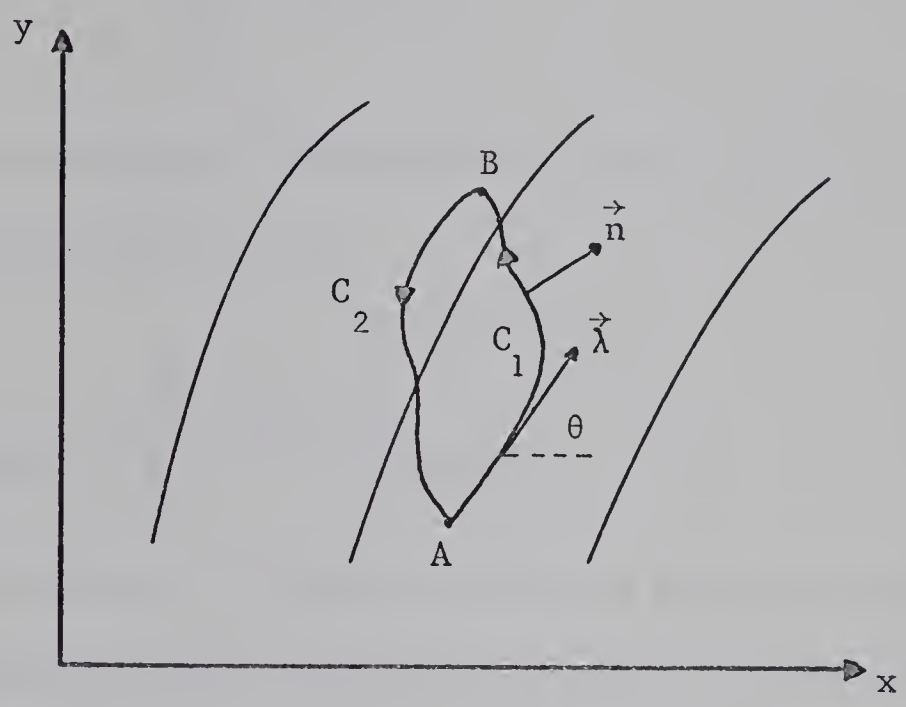

FIGURE (2-1) Streamlines for a two-dimensional flow (after Whitaker, 1968).

Figure (2-1) illustrates the streamlines for a two-dimensional flow and an arbitrary closed curve along which an integration will be performed to define the stream-function.

The mass flow rate across the section C_1 of the curve from A to B is given by

$$\int_A^B \rho \, \vec{V} \cdot \vec{n} \, ds \, , \qquad (2\text{-}3)$$

where ρ is the density per unit horizontal area, $\vec{V}$ the velocity, $\vec{n}$ a

unit vector normal to the path, and ds an element of distance along the path. Similarly, the mass flow rate across the line C_2 from B to A is given by

$$\int_B^A \rho \, \vec{V}\cdot\vec{n} \, ds \, . \qquad (2\text{-}4)$$

Since the mass in the region, bounded by the curves C_1 and C_2, is constant for an incompressible fluid, then

$$\int_A^B \vec{V}\cdot\vec{n} \, ds \Big|_{\text{along } C_1} + \int_B^A \vec{V}\cdot\vec{n} \, ds \Big|_{\text{along } C_2} = 0 \, , \qquad (2\text{-}5)$$

where the constant density, ρ, has been removed from the equation. Changing the direction of the integration along C_2, equation (2-5) becomes

$$\int_A^B \vec{V}\cdot\vec{n} \, ds \Big|_{\text{along } C_1} = \int_A^B \vec{V}\cdot\vec{n} \, ds \Big|_{\text{along } C_2} \, . \qquad (2\text{-}6)$$

Therefore, the integral is independent of the path and, consequently, $\vec{V}\cdot\vec{n} \, ds$ is an exact differential of a function ψ such that

$$d\psi = \vec{V}\cdot\vec{n} \, ds \, . \qquad (2\text{-}7)$$

The function ψ, called the stream-function, is independent of the path linking the points A and B. When $d\psi$ is expressed as a function of the space coordinates x and y and the right hand side of equation (2-7) is expanded, it becomes

$$\left(\frac{\partial\psi}{\partial x}\right) dx + \left(\frac{\partial\psi}{\partial y}\right) dy = u n_x ds + v n_y ds \, , \qquad (2\text{-}8)$$

where u, v, and n_x, n_y are the x and y components of $\vec{V}$ and $\vec{n}$, respectively.

If $\vec{\lambda}$ is a unit vector tangent to an arbitrary curve, then

$$\vec{\lambda} = |\vec{\lambda}| \cos\theta \vec{i} + |\vec{\lambda}| \sin\theta \vec{j} , \qquad (2\text{-}9)$$

where θ is the angle $\vec{\lambda}$ makes with the x-axis (see Figure (2-1)). It is easily seen that

$$\cos\theta = \frac{dx}{ds} , \qquad (2\text{-}10)$$

and

$$\sin\theta = \frac{dy}{ds} . \qquad (2\text{-}11)$$

Equation (2-9) becomes

$$\vec{\lambda} = \frac{dx}{ds}\vec{i} + \frac{dy}{ds}\vec{j} \qquad (2\text{-}12)$$

because $|\vec{\lambda}|$ is unity. Since $\vec{n}$ is normal to the arbitrary curve, the scalar product

$$\vec{n}\cdot\vec{\lambda} = n_x \frac{dx}{ds} + n_y \frac{dy}{ds} = 0 . \qquad (2\text{-}13)$$

Therefore,

$$n_x = -\frac{dy}{ds} , \quad n_y = \frac{dx}{ds} , \qquad (2\text{-}14a)$$

or

$$n_x = \frac{dy}{ds} , \quad n_y = -\frac{dx}{ds} . \qquad (2\text{-}14b)$$

Both equations (2-14a) and (2-14b) satisfy equation (2-13). The difference between the two depends on the direction assigned to $\vec{\lambda}$. Let us choose $\vec{\lambda}$ in such a way that equation (2-14a) will apply. After the substitution for n_x and n_y, equation (2-8) becomes

$$\left(\frac{\partial\psi}{\partial x} - v\right) dx + \left(\frac{\partial\psi}{\partial y} + u\right) dy = 0 . \qquad (2\text{-}15)$$

Since this result is true for any arbitrary curve, the values of dx and dy being arbitrary implies that the terms in each parenthesis must be zero. Hence,

$$u = -\frac{\partial \psi}{\partial y} , \tag{2-16a}$$

$$v = \frac{\partial \psi}{\partial x} , \tag{2-16b}$$

and the velocity components of the flow may be obtained from a stream-function. The existence of a stream-function for two-dimensional, incompressible flow is thus established, and the velocity components must satisfy equations (2-16a) and (2-16b).

Because $d\psi$ is an exact differential, equation (2-7) can be written

$$\psi_B - \psi_A = \int_A^B d\psi = \int_A^B \vec{V} \cdot \vec{n} \, ds . \tag{2-17}$$

If the points A and B lie on a streamline, the integration may be performed along the streamline itself. In this case

$$\vec{V} = |\vec{V}| \, \vec{\lambda} . \tag{2-18}$$

Equation (2-17) becomes

$$\psi_B - \psi_A = \int_A^B |\vec{V}| \, \vec{\lambda} \cdot \vec{n} \, ds = 0 \tag{2-19}$$

by equation (2-13). Therefore,

$$\psi_B = \psi_A$$

and it may be concluded that the value of ψ is constant along any streamline.

From the equation of continuity

$$-\frac{1}{\rho}\frac{d\rho}{dt} = \text{Div}\ \vec{V}\ , \qquad (2\text{-}20)$$

it is seen that the atmosphere may be treated as if it were incompressible if the divergence is zero, or negligibly small. In addition, if the flow above the friction layer is considered, then equations (2-16a) and (2-16b) would be the geostrophic wind relationship. Along with equation (2-19) it could be used to describe the isobaric flow at a particular pressure level.

CHAPTER III

COMPUTATION OF THE STREAM-FUNCTION AT STATIONS AND AT GRID POINTS

Introduction

A direct method of fitting a stream-function ψ to the wind observations at stations has been described by Endlich and Mancuso (1964). They wanted to use it as a possible replacement for the operational streamline-isotach analyses in the tropics. A year later, Endlich and Mancuso (1965) modified and improved this technique for application to upper-air data over the United States. In addition, the new technique contains an objective analysis to compute the stream-function values at the points of a grid using the observed values of height and wind at radiosonde stations.

It is realized, of course, that more sophisticated methods of objective analysis could have been used. To mention just a few, there is Cressman's correction method (Cressman, 1959), Grandin's method of optimal extrapolation (Grandin, 1963), and the methods of polynomial interpolation such as that of quadric fitting described by Bushby and Huckle (1957). These methods require storage facilities and computational procedures that can be handled efficiently only by large, specialized computers such as are available in a central meteorological facility. A simpler approach was followed in this study to avoid the complications of large storage and long running times.

The objective analysis used has the advantage of yielding the streamlines directly by analyzing the stream-function values without additional computations. It avoids problems relating to climatological

data access and extensive computations. Furthermore, it does not require boundary conditions. This is important, for Hawkins and Rosenthal (1965) have shown that the results obtained by solving a Poisson equation to get the stream-function were very much dependent on the choice of boundary conditions. Agnew (1969) used the simplified method to calculate streamlines in the eastern United States and showed that this approach yielded worthwhile results. It was hence decided to apply this method also to the problem of orographic flow in the Canadian Rocky Mountains.

Stream-Function at Stations

The method is based on the formulation of the stream-function differential $d\psi$ between two nearby points separated by space differentials dx and dy as

$$d\psi = \left(\frac{\partial\psi}{\partial x}\right) dx + \left(\frac{\partial\psi}{\partial y}\right) dy \ . \qquad (3\text{-}1)$$

As mentioned in Chapter II, the geostrophic wind is related to the stream-function by

$$\vec{V} = \vec{k} \times \vec{\nabla}\psi \ , \qquad (3\text{-}2)$$

the vector equivalent to equations (2-16a) and (2-16b). Substituting for $\frac{\partial\psi}{\partial x}$ and $\frac{\partial\psi}{\partial y}$, equation (3-1) becomes

$$d\psi = v dx - u dy \ . \qquad (3\text{-}3)$$

This equation can be written in finite difference form as

$$\Delta\psi = v\Delta x - u\Delta y \ . \qquad (3\text{-}4)$$

The dimensions of the stream-function ψ are $[L^2T^{-1}]$ from equation (3-2). In this dimensional form the stream-function cannot

be directly compared with any other meteorological quantity. For the purpose of comparing values of the stream-function with observed heights, it is convenient to define a new function

$$\overset{*}{\psi} = \frac{f}{9.8}\psi \ , \qquad (3\text{-}5)$$

where f is the Coriolis parameter.

The geostrophic wind is also related to the contour height by

$$\vec{V} = \frac{9.8}{f}\vec{k} \times \vec{\nabla}Z \qquad (3\text{-}6)$$

when Z is measured in geopotential meters. Equations (3-2) and (3-6) imply that, if the flow were geostrophic, then

$$\Delta\overset{*}{\psi} = \Delta Z \ . \qquad (3\text{-}7)$$

Substituting (3-5) in equation (3-3) leads to

$$\Delta\overset{*}{\psi} = \frac{f}{9.8}(v\Delta x - u\Delta y) \ . \qquad (3\text{-}8)$$

$\Delta\overset{*}{\psi}$ between a particular station o and a nearby station i is

$$\Delta\overset{*}{\psi}_i = \overset{*}{\psi}_o - \overset{*}{\psi}_i \ ,$$

where the origin is taken to be at station i.

Therefore,

$$\overset{*}{\psi}_o = \overset{*}{\psi}_i + \Delta\overset{*}{\psi}_i \ . \qquad (3\text{-}9)$$

An estimate of $\Delta\overset{*}{\psi}_i$ may be acquired by a weighted combination of winds and heights using equations (3-7) and (3-8). The weighted equation is written in a general form as

$$\Delta\overset{*}{\psi}_i = \frac{\bar{f}}{9.8}\left[(\omega_1 v_o + \omega_2 v_i)(x_o - x_i) - (\omega_1 u_o + \omega_2 u_i)(y_o - y_i)\right] + \omega_3(Z_o - Z_i) \quad (3\text{-}10)$$

where ω_1, ω_2, ω_3 are weighting factors with empirically determined values (Endlich and Mancuso, 1965) of 0.45, 0.45, and 0.1, respectively. $\bar{f}$ is the mean Coriolis parameter given by

$$\bar{f} = \frac{f_o + f_i}{2}$$

Estimates of $\overset{*}{\psi}_o$ can be obtained with respect to each of its nearby neighbors, i = 1, 2, 3, ..., n. A reasonable value of $\overset{*}{\psi}_o$ might be taken as the average of the individual estimates. That is

$$\overset{*}{\psi}_o = \frac{1}{n}\sum_{i=1}^{n}(\overset{*}{\psi}_i + \Delta\overset{*}{\psi}_i) \quad . \quad (3\text{-}11)$$

Two estimates of $\overset{*}{\psi}_o$ are computed in the stream-function routine. The first, $(\overset{*}{\psi}_o)_1$, considers all stations lying within a radius[1] of 300 miles from station o. A second estimate, $(\overset{*}{\psi}_o)_2$ considers all stations lying between a radius of 300 and 550 miles from station o. The two estimates are combined to give the better approximation:

$$\overset{*}{\psi}_o = \mu_1(\overset{*}{\psi}_o)_1 + \mu_2(\overset{*}{\psi}_o)_2 \quad . \quad (3\text{-}12)$$

Here μ_1 and μ_2 are weighting factors (Endlich and Mancuso, 1965) with values of 0.8 and 0.2, respectively.

---

[1] All radii used in this study are taken to be the great-circle distance between the two stations.

The reported contour heights are used as the initial estimate of $\overset{*}{\psi}_i$ at each station since they are a reasonably accurate and very convenient first guess. Then, the entire field of stations is scanned, and new values of $\overset{*}{\psi}_o$ are computed using equations (3-10), (3-11), and (3-12). The new estimates of $\overset{*}{\psi}_o$ are then back-substituted into the computation equations, much as in a Liebmann iteration (see Butler and Kerr, 1962) until a convergence within a prescribed limit is reached.

A total of fifteen iterations were used in this study mainly because the convergence in data-sparse zones was slow. Although a change in the value of $\overset{*}{\psi}_o$ within five geopotential meters (gpm)[1] would have been considered reasonable in these critical areas, a general convergence within 2 gpm could be obtained with fifteen scans. However, in the dense data regions, $\overset{*}{\psi}_o$ converged readily to within one gpm. Furthermore, a total of thirty-five iterations produced a convergence everywhere within one gpm.

The computed values of $\overset{*}{\psi}_o$ were adjusted so that their average value is equal to the mean of the 850-mb heights. The adjustment was made in order to overcome some of the errors introduced by this method, especially when a few stations are located within the scanning radii of a station. The correction is done as follows:

$$\overset{*}{\psi}_o = \overset{*}{\psi}_o \times \frac{\text{Average of 850-mb heights}}{\text{Average of } \overset{*}{\psi}_o \text{ over the area}} . \qquad (3\text{-}14)$$

Objective Analysis

After $\overset{*}{\psi}_o$ has been computed at each of the stations, the

[1] The abbreviation gpm will be used to denote geopotential meters.

stream-function values are then calculated at the points of a grid which is used to permit a more detailed look at the situation, for station data alone are usually inadequate to define the flow pattern in the mountains.

The technique of objective analysis at grid points uses many of the features of the computation of $\overset{*}{\psi}_o$ at stations. A value of the stream-function $\overset{*}{\psi}$ at a particular grid point ℓ may be estimated from values at nearby stations i by the relation:

$$\overset{*}{\psi}_\ell = \overset{*}{\psi}_i + \Delta\overset{*}{\psi}_i \,, \qquad (3\text{-}15)$$

where

$$\Delta\overset{*}{\psi}_i = \frac{\bar{f}}{9.8}\left[v_i(x_\ell - x_i) - u_i(y_\ell - y_i)\right] \,. \qquad (3\text{-}16)$$

$\bar{f}$ is again the mean Coriolis parameter which, in this case, is

$$\bar{f} = \frac{f_\ell + f_i}{2} \,.$$

If there are n stations near the grid point ℓ, the desired value is an average of the n estimates. Therefore,

$$\overset{*}{\psi}_\ell = \sum_{i=1}^{n} \gamma_i \left(\overset{*}{\psi}_i + \Delta\overset{*}{\psi}_i\right) \Big/ \sum_{i=1}^{n} \gamma_i \,, \qquad (3\text{-}17)$$

where γ_i is a weighting factor to be discussed later.

As before, two estimates of $\overset{*}{\psi}_\ell$ are found. $(\overset{*}{\psi}_\ell)_1$ is evaluated using stations within 240 miles from the grid point. $(\overset{*}{\psi}_\ell)_2$ is estimated using stations between 240 and 500 miles from the grid point. These two values are combined to give a best estimate using weighting factors of 0.9 for the inner scan and 0.1 for the outer scan. That is,

$$\overset{*}{\psi}_{\ell} = 0.9\ (\overset{*}{\psi}_{\ell})_1 + 0.1\ (\overset{*}{\psi}_{\ell})_2 \ . \qquad (3\text{-}18)$$

The weighting factor γ_i is defined to be

$$\gamma_i \equiv \frac{C}{C + |\Delta\overset{*}{\psi}_i|} \ , \qquad (3\text{-}19)$$

where C is an arbitrary constant. It is set equal to the average value of $|\Delta\overset{*}{\psi}_i|$ for the 13 stations within the inner scanning radius of Lethbridge (QL), a station with a high number of neighbors.

A closer look at γ_i shows that it tends toward unity when $|\Delta\overset{*}{\psi}_i|$ is small. Such situations occur when:

(a) stations are relatively near the grid point.

(b) stations are large distances upstream or downstream from the grid point but on or near the same streamline.

The method just described is applied to a grid[1] lying over the Canadian Rocky Mountains. When $\overset{*}{\psi}$ has been calculated at all the grid points, streamlines can be drawn simply by joining identical values of the stream-function.

---

[1] Details about the grid will be given in Chapter IV.

CHAPTER IV

TERRAIN-INDUCED VERTICAL VELOCITIES AND THE HEIGHT PROFILE

Introduction

Since this study considers only large scale flow, influences of terrain on small scales of atmospheric motion such as the generation of gravity waves by mountains are not considered. It is well recognized that mountain-induced vertical motions associated with the phenomenon of mountain waves extend to very great heights, even up into the mesosphere. Such processes have, however, not yet been observed on a synoptic scale (see McClain, 1960).

For the purpose of finding orographic vertical velocities, it is first assumed that the airstream in the lower atmosphere follows essentially the relief of the terrain. This is a reasonable and almost universal assumption used in most formulations of numerical models incorporating orographic effects.

Terrain-Induced Vertical Velocities

Let H (I, J) represent the height of the terrain at grid point (I, J). Since the airstream is assumed to follow the relief of the ground, the vertical component of the wind is equal to the product of the horizontal component of the wind and the tangent of the angle of inclination of the slope. A look at a simple two-dimensional case will clarify the above statement.

Consider Figure (4-1) which illustrates the cross-section of

a mountain, and a wind $\vec{V}$ with a horizontal component $\vec{V}_h$ and a vertical component $\vec{w}$. That is,

$$\vec{V} = \vec{V}_h + \vec{w} \ . \qquad (4\text{-}1)$$

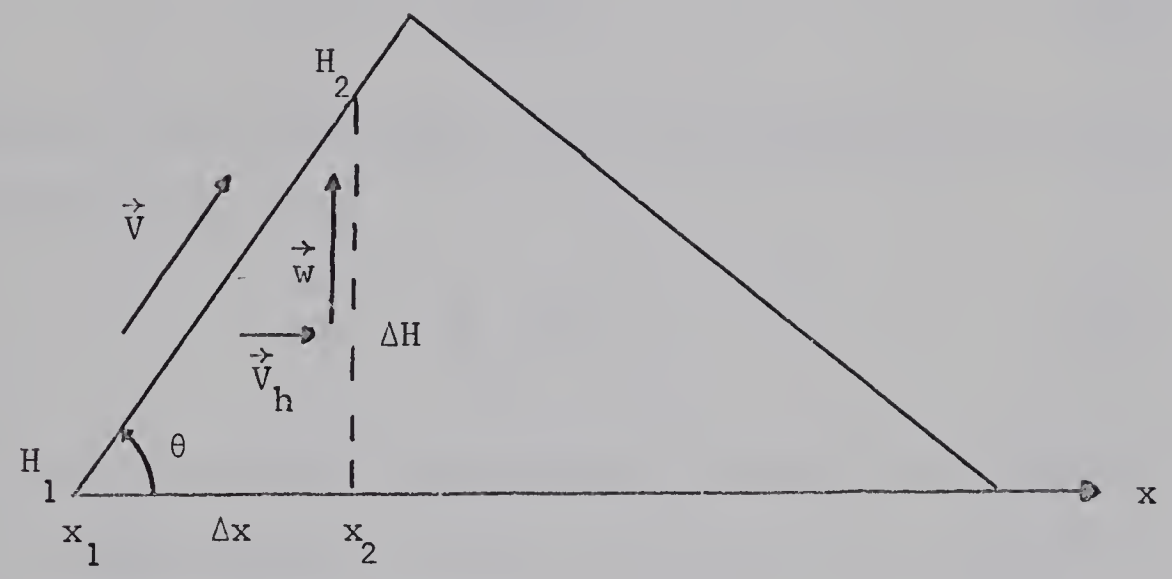

FIGURE (4-1) Cross-section of a mountain ridge showing the wind $\vec{V}$ blowing along the slope, and the respective horizontal and vertical components $\vec{V}_h$ and $\vec{w}$. θ is the angle of inclination. H_1 and H_2 are heights of the terrain at two arbitrary points along the slope.

With $\Delta x = x_2 - x_1$, the magnitude of the gradient of H, $|\vec{\nabla H}|$, can be written

$$|\nabla H| = \frac{\Delta H}{\Delta x} = \tan\theta \ . \qquad (4\text{-}2)$$

But in this case, tan θ is also related to the ratio of the wind components,

$$\tan \theta = \frac{|\vec{w}|}{|\vec{V}_h|} = \frac{w}{V_h} \quad . \qquad (4\text{-}3)$$

Therefore,

$$w = V_h \tan \theta \quad , \qquad (4\text{-}4)$$

and, by equation (4-2),

$$w = V_h \frac{\partial H}{\partial x} \quad . \qquad (4\text{-}5)$$

For the general three-dimensional case, the expression for the vertical wind is readily shown to be

$$w = \vec{V}_h \cdot \vec{\nabla} H \quad . \qquad (4\text{-}6)$$

Values of w computed in this way will most likely be too large in the vicinity of higher obstacles, for it is a known fact that part of the flow is diverted around the barriers.

Because the 850-mb level is usually some distance above the ground, a criterion needs to be established to determine to what extent the flow at this level is affected by an obstacle below. As a theoretical approach to this problem, consider Figure (4-2) which represents the flow round a half cylinder of radius A in a stream of velocity U. The stream-function for this type of potential flow is given in most texts of fluid mechanics. The resulting equation, in polar coordinates, can be shown to be:

$$\psi = -U \left(r - \frac{A^2}{r}\right) \sin \theta \quad , \qquad (4\text{-}7)$$

where U is the wind at an infinite distance from the obstacle, A the radius of the cylinder, r the radial distance to any point p, and θ the angle the radius vector r makes with the positive x-axis.

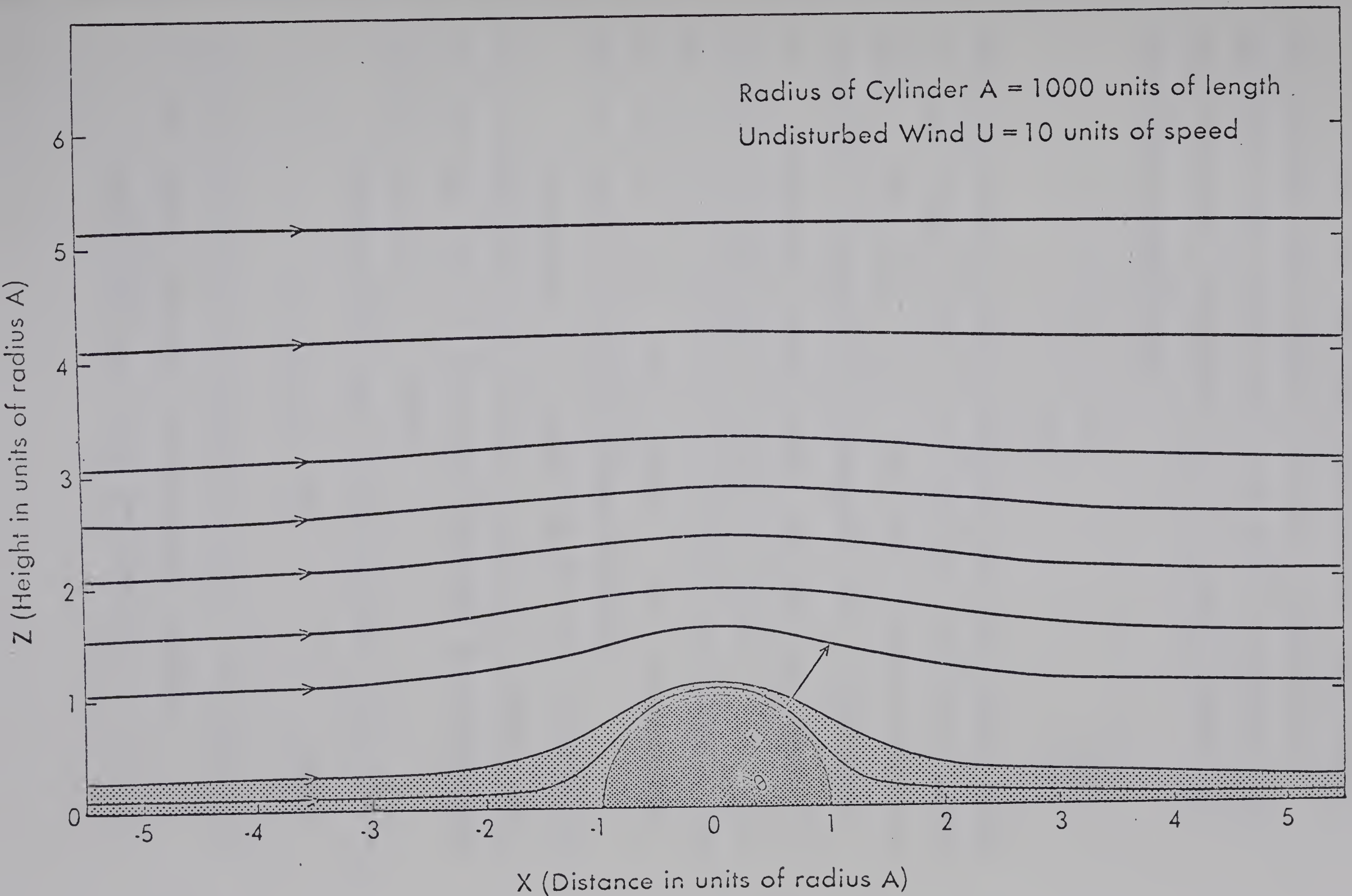

FIGURE (4-2) Potential flow past a half cylinder of radius A in a stream of undisturbed velocity U. Shaded area represents a mountain barrier; r and θ are the polar coordinates.

Since U and A are known, equation (4-7) is used in order to plot a curve for various values of constant ψ. A value of r is computed for each θ between zero and 180 degrees. Furthermore, each computed value of r is converted to the x-z coordinate system using the following transformations:

$$x = r \cos \theta \,, \qquad (4\text{-}8)$$

$$z = r \sin \theta \,. \qquad (4\text{-}9)$$

Figure (4-2) shows the result of plotting x and z for different values of ψ using U equal to 10 meters per second, and a cylindrical obstacle radius A of 1000 meters. Each of these curves represents a streamline; consequently, by definition of a streamline, anyone of them could be used as an appropriate barrier profile. The shaded area (Figure (4-2) indicates the profile chosen to represent the obstacle. It is evident that the streamlines show decreases in amplitude and steepness of slope with increasing distance from the obstacle. Soon a level is reached where the influence of the barrier becomes negligible.

More generally, it is agreed that the effect of the terrain on the flow decreases with distance from the terrain boundary. However, the exact nature of the fall-off with height of terrain-induced vertical velocities is still unknown.

Graystone (1962) used a parabolic decrease. His expression is

$$w = \frac{1}{4} w_o \, (1 - \alpha^*)^2 \,, \qquad (4\text{-}10)$$

where w_o is the terrain-induced vertical velocity at the surface, and α^* is the vertical coordinate linearly related to pressure.

Estoque (1957) used a power law of the form

$$w = w_{p_o} \left(\frac{p}{p_o}\right)^b \quad , \tag{4-11}$$

where b has a value between 2 and 3, p_o is equal to 1000 mb, and p is the pressure at the level considered. Reuter and Pichler (1964) used a similar power law but with the exponent b = 4.

Murakami (1956) chose the decrease to be exponential in his model. He used

$$w = w_{p_o} \frac{\sinh \alpha p}{\sinh \alpha p_o} \quad , \tag{4-12}$$

where

$$\alpha^2 = \frac{4\,g}{d^2 k f^2} \quad , \tag{4-13}$$

p_o is the pressure at the ground, p the pressure at the level of interest, d the horizontal mesh size, f the Coriolis parameter, and k is equal to

$$1 \Big/ \frac{\partial z}{\partial p} \frac{\partial \ln\theta}{\partial p} \quad ,$$

where θ is the potential temperature.

McClain (1960) did a study of the Western Cordillera. From a survey of equivalent potential temperature trajectories and also from the configuration of isentropic surfaces represented on a cross-section taken across the mountains he observed that the level where the terrain influence is negligible lies somewhere in the first few kilometers above the mountain slopes. He suggested this level to be about three kilometers above the terrain.

Smagorinsky and Collins (1955) used a linear law for the decrease of terrain-induced vertical velocities in their quantitative

precipitation model. Their reason for this choice is made clear in the following quotation:

> While this procedure is somewhat arbitrary, it has the characteristic, somewhat similar to the atmosphere, that the effects of the lower boundary on the flow are damped out approximately linearly with decreasing pressure.

Because this hypothesis seemed reasonable, it was decided that as a first approximation, a linear decrease of w to zero at three kilometers above the terrain would be used in this study. A linear decrease with height is readily incorporated into equation (4-6) by the inclusion of a parameter K whose value varies according to the distance of $\overset{*}{\psi}$ above the barrier. This is one reason why $\overset{*}{\psi}$ was analyzed instead of ψ itself[1]. With this modification

$$w = K\,(\vec{V}_h \cdot \vec{\nabla} H) \quad . \qquad (4\text{-}14)$$

The horizontal wind $\vec{V}_h$ can be found from the stream-function gradient by using the centered finite difference method of approximating partial differential equations. The grid points involved are arranged in the following way:

---

[1] If the assumption is made that 1 gpm ≈ 1 meter.

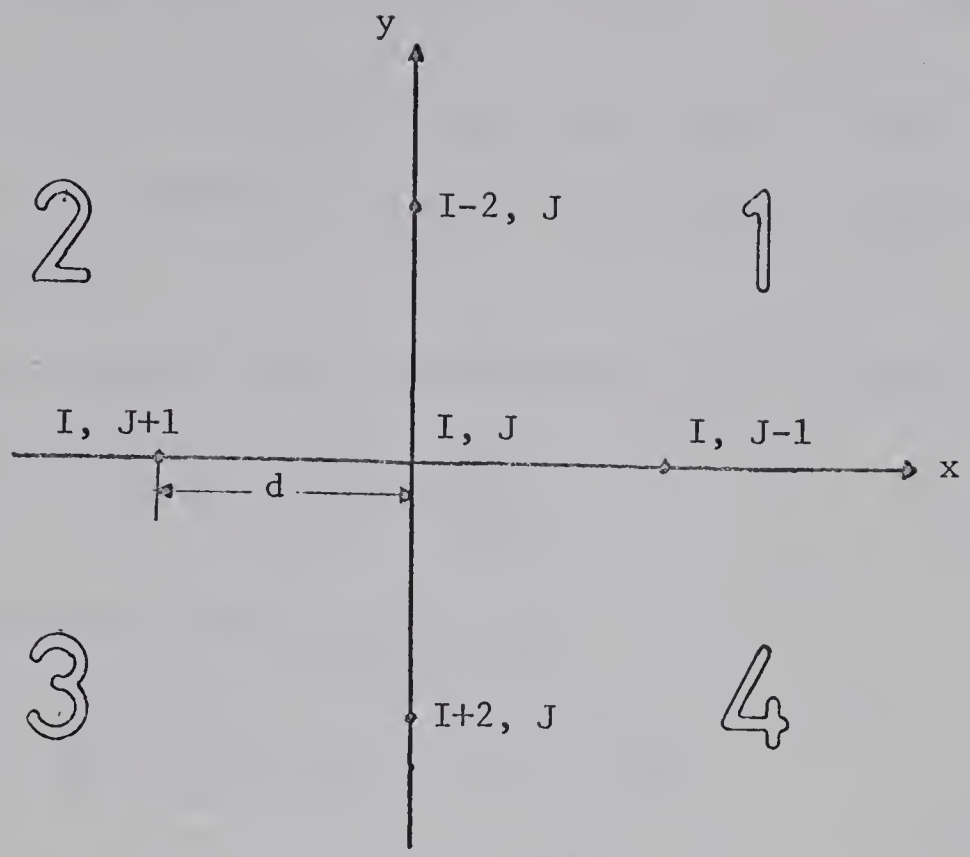

FIGURE (4-3) Grid point configuration used in the finite difference scheme to solve partial differential equations. d is the mesh size, and the numbers 1-4 refer to quadrants. The indices shown refer exactly to those used in all computations.

Since the components of $\vec{V}_h$ are from equations (3-2) and (3-5)

$$u = -\frac{9.8}{f}\frac{\partial \overset{*}{\psi}}{\partial y},$$

and

$$v = \frac{9.8}{f}\frac{\partial \overset{*}{\psi}}{\partial x},$$

they become in finite difference form using the system in Figure (4-3),

$$u(I, J) = -\frac{9.8m}{2df}\left[\overset{*}{\psi}(I-2, J) - \overset{*}{\psi}(I+2, J)\right], \qquad (4\text{-}15)$$

and

$$v(I, J) = + \frac{9.8m}{2df} \left[\overset{*}{\psi}(I, J-1) - \overset{*}{\psi}(I, J+1) \right] , \qquad (4\text{-}16)$$

where f is the Coriolis parameter at grid point (I, J), d the grid length, and m the map factor[1] for a polar stereographic projection true at latitude 60°N.

Writing equation (4-14) in component form, it becomes

$$w = K \left(u \frac{\partial H}{\partial x} + v \frac{\partial H}{\partial y} \right) . \qquad (4\text{-}17)$$

In finite difference form this equation is

$$w = \frac{Km}{2d} \left[u \left(H(I, J-1) - H(I, J+1) \right) + v \left(H(I-2, J) - H(I+2, J) \right) \right] . \qquad (4\text{-}18)$$

Some difficulty is encountered with the above equation when H(I, J) is the height of a mountain peak which is entirely below the surface of $\overset{*}{\psi}$, a situation which will be referred to as a "low peak".

The present centered finite difference scheme would not be representative because the calculated average slope would normally be less than the two slopes defining the peak. It can be easily seen from Figure (4-4) that a centered finite difference approximation would give a false representation of the actual slopes. To get a more realistic slope, the direction from where the wind is blowing is determined from the sign of the wind components u and v. Then, the differences between H(I, J) and the height of each of the other two grid points involved are used to represent the slope.

The wind $\vec{V}_h$ is not given special consideration because the slope of a pressure surface is known to be small. Referring to Figure (4-4),

---

[1] See Appendix B for the derivation of this map factor.

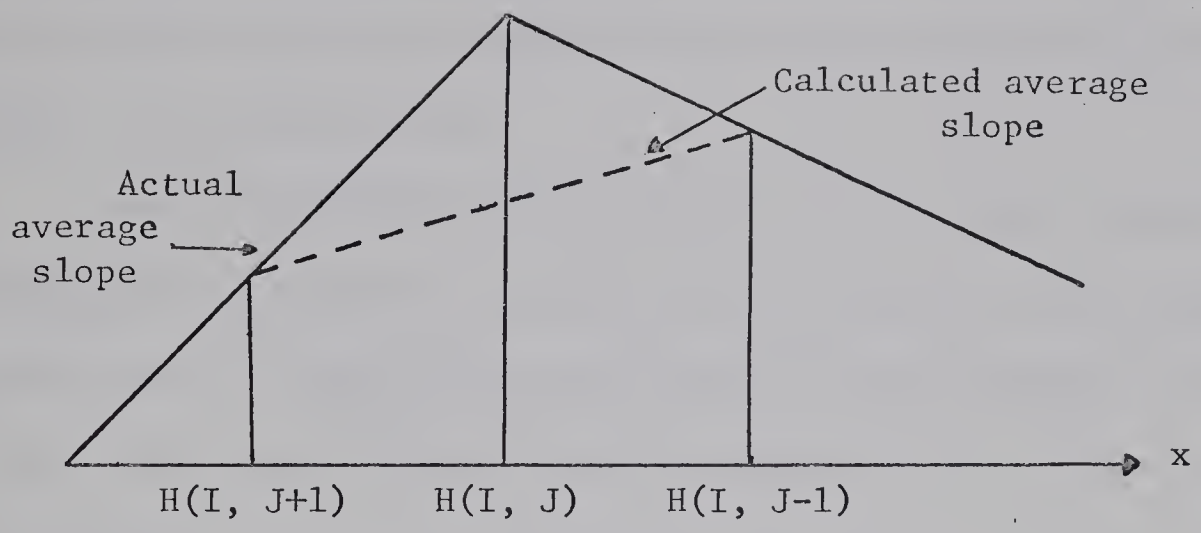

FIGURE (4-4) Cross-section of a low peak showing the actual average slope (solid line) and the slope (broken line) brought out by finite difference methods.

this means that the slope of the pressure surface between grid points (I, J-1) and (I, J+1) is the same as between grid points (I, J) and (I, J+1).

To illustrate this problem further, let us suppose that u and v are both positive. Then the wind is blowing from the third quadrant (see Figure (4-3)). The expression for w, using the notation in Figure (4-3) would be

$$w = \frac{Km}{d}\left[u(H(I, J) - H(I, J+1)) + v(H(I, J) - H(I+2, J))\right] , \quad (4\text{-}19)$$

where the symbols have the same meaning as defined previously.

The mountain ridges are handled in the same manner. The criterion used in this case is: If H(I, J) is greater than either one of the other two heights involved (depending on wind direction), an

equation similar to (4-19) is used in the vertical wind computation. Since the values of w are stored at grid point (I, J), which is a peak or the crest of a ridge, it is kept in mind that the value applies slightly upwind from these highest points where theoretically the orographic influence is zero.

Basins and intermountain valleys are not given special considerations because the centered-difference method most likely represents what is happening under synoptic flow conditions. Cook and Topil (1952) make reference to that effect in an article about chinook winds:

> Pilots on flights over the San Luis Basin in southern Colorado report that warm air during Chinook conditions does not enter even the larger intermountain valleys. This Basin is bounded by the Continental Divide on the west and the Sangre de Cristo Range on the east, the crests of the ranges being about 70 miles apart across the valley. The pilots state that when strong westerly winds of chinook type blow across the valley above the level of the tops of the ranges, very little wind or turbulence is found below the level of the tops. However, a downdraft is encountered on the east side of the Sangre de Cristo Range where the wind descends to the Great Plains.

This situation is represented in the following diagram, Figure (4-5). The broken line represents the slope used in the calculations. It is seen to be much less than the actual slope. The downdraught at grid point (I, J) would thus be reduced for a wind blowing across the valley.

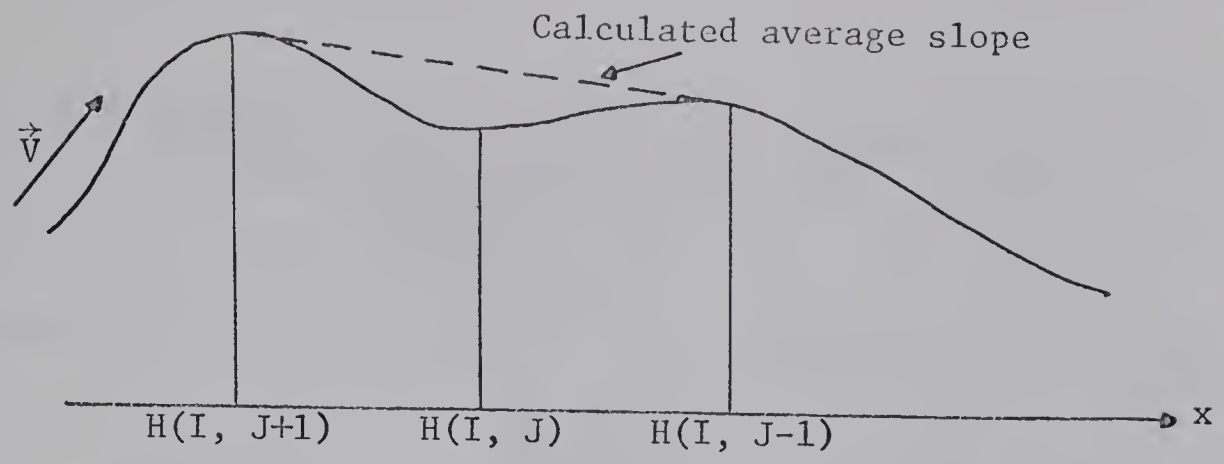

FIGURE (4-5) Cross-section along the x-axis of a mountain valley showing the actual slope (solid line) and the slope used in the computations (broken line).

The Grid

A 35 × 28 grid covering the area shown in Figure (4-6) is used. The orientation of this grid has the advantage that its columns are directed along the Rocky Mountains, and is such that, if the grid were extended to the east, one of its columns would coincide with 80°W meridian of the USWB standard grid (see Figure (4-6)).

The mesh size thought to be fine enough to preserve a good representation of the height profile is 95.25 kilometers, which is one-quarter of the standard grid length of 381 kilometers used operationally in numerical weather prediction. Since the method described utilizes discrete grid points, an averaging process has to be performed so that H(I, J) represents adequately the area surrounding the grid point.

The Height Profile

The height of the terrain of every "one-eighth" grid point[1]

[1] One-eighth grid points are separated by intervals equal to one eighth the standard grid length of 381 km.

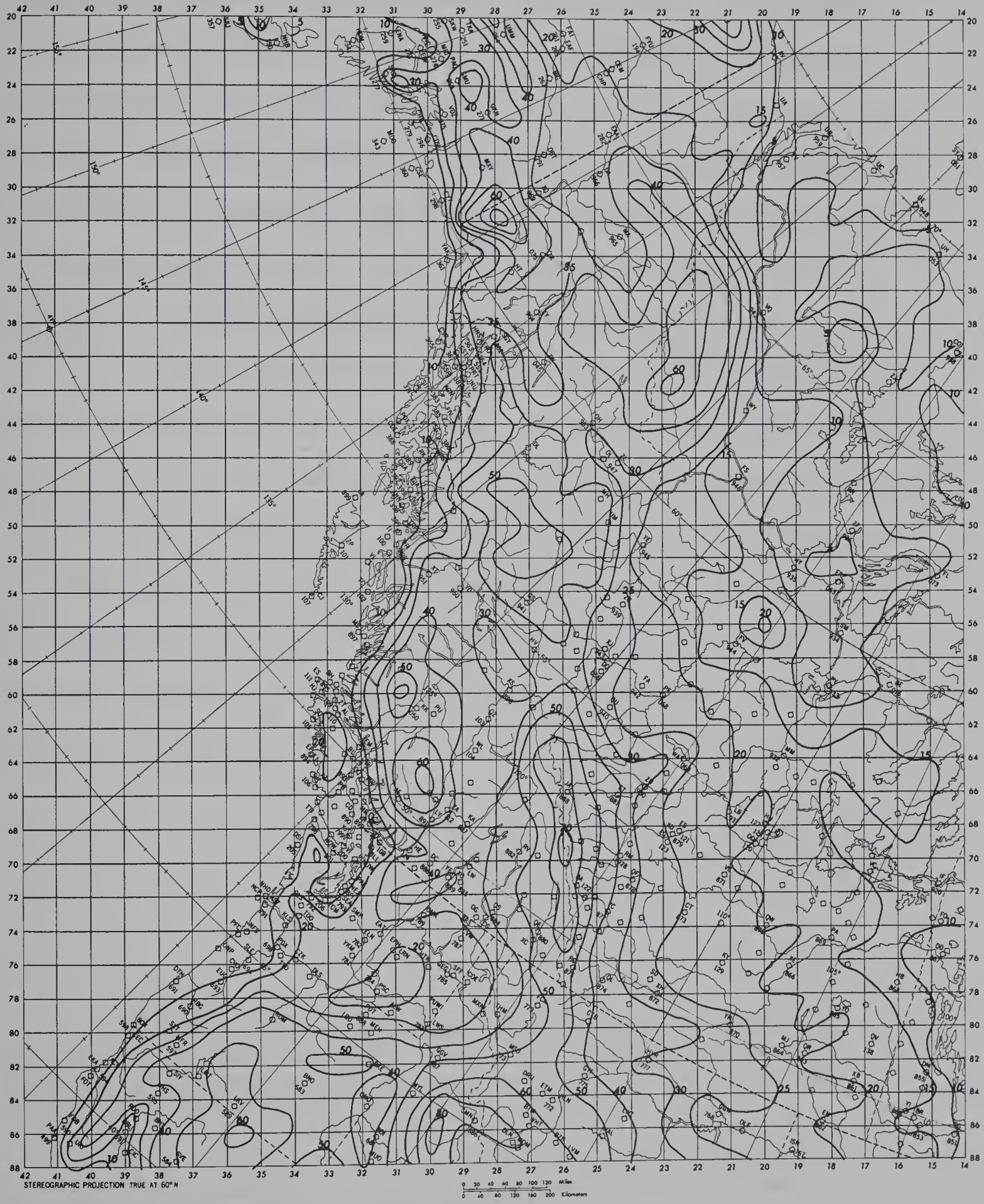

FIGURE (4-6) Smoothed height profile of the area covered by the one-quarter grid (95.25 km grid length). Contours labelled in hundreds of feet are drawn at intervals of 1000 feet M.S.L. in rough terrain and at 500 feet in smooth areas.

was found on topographic maps[1] of scale 1:250,000. On this scale contours are drawn at intervals ranging from 100 feet in relatively flat areas to 500 feet in rough terrain. The process is simple but time-consuming. After the geographic coordinates of each point are computed[2], they are located on the topographic map and the height is interpolated if necessary. The numbering system for rows and columns on the actual grid is such that it facilitates the calculation of geographic coordinates which is started from the North Pole.

It is thought that the height found at each one-quarter grid point has to be given more weight than the neighbouring heights because it is more directly involved in the computations. Therefore, the height at one-quarter grid point is given a weight of 0.4 and the mean of the surrounding one-eighth grid points is given a weight of 0.6. The resulting height is the H(I, J) value used in the calculations. The following diagram illustrates the system of grid points used for one averaging process.

---

[1] Topographic series produced and printed in Canada by the Surveys and Mapping Branch, Department of Energy, Mines and Resources, Government of Canada, and in the United States by the Interior Geological Survey, Washington, D.C.

[2] See Appendix B for the procedure involved in the calculation of geographic coordinates.

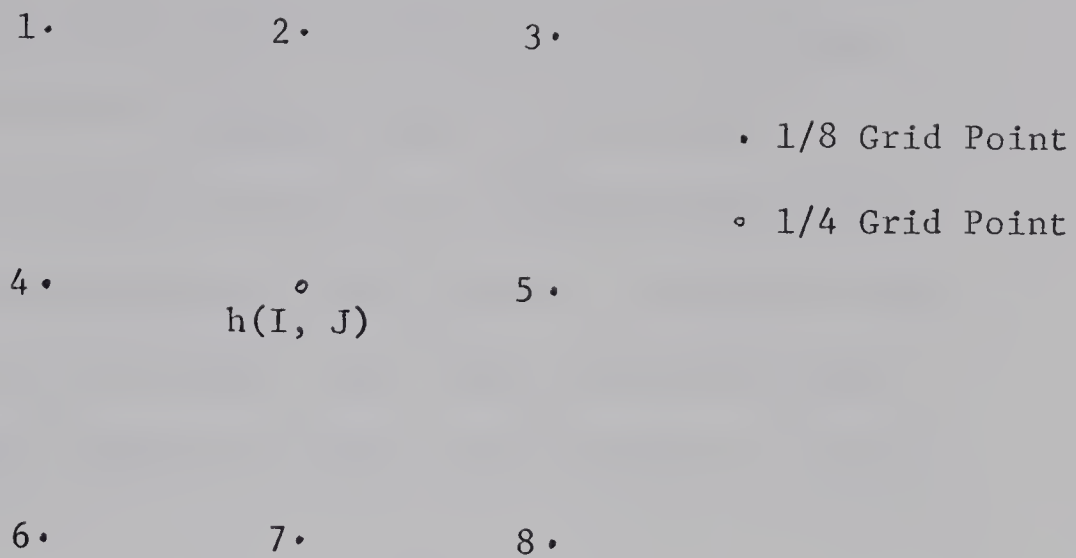

$$H(I, J) = \left[\frac{1}{8}(h_1 + h_2 + h_3 + h_4 + h_5 + h_6 + h_7 + h_8)\right] \times 0.6$$

$$+ h(I, J) \times 0.4$$

FIGURE (4-7) System of grid points used in averaging process. Points numbered from 1 to 8 represent 1/8 grid points and the central point, a 1/4 grid point. h refers to observed height.

However, the height of the terrain at only one-quarter grid points is used to calculate representative heights in the areas to the right of column nineteen in Figure (4-6) because the terrain is quite smooth in this part of the region. The geographic coordinates plus the corresponding average height for each one-quarter grid point are given in Appendix A. The resulting smoothed profile shown in Figure (4-6) still brings out the synoptically important features. Four significant features can be easily recognized:

(a) The major ranges are still well defined and stand out clearly.

(b) The major passes and passages for air are located at latitude 60°N, between the Stikine Mountains to the south and the

Mackenzie to the north; and at latitude 55°N between the Stikine Mountains to the north and the Alberta Range to the south.

(c) The only complete barrier to the 850-mb flow is the Alberta Range which extends from the 55°N parallel, southward along the Alberta-British Columbia border, and, thence, into the United States where the highest ground is found, and the barrier broadens considerably.

(d) The eastern flank of the Cordillera is not nearly as complex as its western part.

This concludes the description of the method used. A network of data points is used to test the performance of the model for flows coming from five different directions over the Canadian Rocky Mountains.

CHAPTER V

EXPERIMENTAL DESIGN

The provinces of British Columbia and Alberta constitute the main area of interest for the purpose of this investigation. However, a grid covering a larger area is used to avoid an abrupt ending of the analyses at the border of the principal domain, and to allow ready extension of the objective analysis to a broader region if necessary and desirable.

The two main regions where data are very sparse are the Pacific Ocean and the Canadian Arctic. The lack of data is most acute over the North Pacific because the only reliable information available at the 850-mb level is from the weather ship Papa (4YP, 50°N, 145°W). This large and synoptically important region, usually upstream from the principal study area, required most often the inclusion of additional data estimates to provide adequate coverage. No data estimates were added in the Arctic and in the area covered by columns 14-20 south of the latitude 60°N (see Figure (4-6)). However, in order to preserve continuity in the analysis over these regions, $\overset{*}{\psi}$ at any location with no neighbors within the distance of the inner scanning radius was simply set equal to Z because, as noted earlier, $\overset{*}{\psi}$ is approximately equal to Z.

The area of the northwestern United States is generally well covered with the existing network of radiosonde stations. Very few estimated data had to be added in the mountainous regions of the U.S. and the objective analysis may be expected to perform well in most of

this area. The mountains of British Columbia create another problem of data because of the small grid length used. The difficulty is to get data estimates conveniently located so that each grid point in the main region has at least two data points within its inner scanning radius.

The estimated data points added in data sparse regions, the radiosonde and pibal stations, and some high level stations[1] where estimates of the height of the 850-mb surface are deduced from surface data, provided a total of 116 points for data input. Some data points, located outside the boundary of the grid, served as neighbors to other data points and to grid points along the border.

Even with such a large number of data points, grid points (30, 24), (30, 25) on the Alaska-Yukon border at latitude 65°N, grid points (66, 15), (68, 15) in northeastern Saskatchewan, and points in the upper left and right hand corners of the grid have no data points within their respective inner scanning radius. In order to preserve the continuity of the analysis, $\overset{*}{\psi}_{\ell}$ at these grid points is simply set equal to the average of the estimates of $\overset{*}{\psi}_{i}$ found within the outer scanning radius. Everywhere else, each grid point has at least one data point within its inner radius and, as mentioned earlier, the number is at least two in the main area.

The input data consist of the wind velocity and the height of the 850-mb level. Missing data are estimated subjectively with the help of the map analysis, neighboring stations, and the surface weather information. The map analyses are generally corrected only for obvious errors but contours were occasionally redrawn to improve an analysis produced, perhaps, too hastily under the stresses of an operational

---

[1] These stations are classified as data estimates in Appendix C.

weather office. However, no attempts were made to modify the analyses significantly over the ocean, because it was felt that the operational meteorologist had a better knowledge of the actual synoptic situation prevailing at the time.

A problem involving the computational roughness in the field of $\overset{*}{\psi}$ caused very strong gradients and, consequently, high wind speeds in some areas of the map. The simplicity of the objective analysis, the sparsity of data, and the rather crude assumptions contributed in a certain way to the problem. Roughness found in the critical areas where the grid points have no data points within their respective inner scanning radii is certainly a result of inadequate data input. They may be classified as "permanent" critical areas because the tight gradients will appear in every case studied. Sometimes, strong gradients were found in areas where it is felt the estimates of $\overset{*}{\psi}_{\ell}$ were based on a sufficient number of data points (2-4 within inner radius). The cause of the roughness is an inherent and general problem of fine-mesh models. Atkins (1970), while working with some of the objective analyses mentioned in Chapter III, on a grid with mesh size of one hundred kilometers for the 10-level Bushby-Timpson model (1967), has experienced a roughness in the field of heights which she attributed to the small grid length. Small-grid fields will require smoothing until better methods of objective analysis have been developed.

Although problems with roughness of field do not arise in the principal regior, other methods of extrapolation to grid points were tried in an attempt to improve the situation in parts of the surrounding area. As a first attempt, the weighting factor γ_i was applied directly to the wind components at data points defined by

$$u_{\ell} = \sum_{i=1}^{n} \gamma_i u_i \Big/ \sum_{i=1}^{n} \gamma_i \qquad (5\text{-}1)$$

and

$$v_{\ell} = \sum_{i=1}^{n} \gamma_i v_i \Big/ \sum_{i=1}^{n} \gamma_i , \qquad (5\text{-}2)$$

where again ℓ refers to grid points and i to neighboring data points.

Although no excessively high wind speeds were encountered in the analysis, a number of other complications arose. The components u_{ℓ} and v_{ℓ}, as found by the above equations, are relative to latitude and longitude positions which are different from the grid coordinates where the equation (4-18) of w is valid. The task of transforming from one system to another is rather involved and tedious: the angle between longitude lines and grid lines, for example, varies with latitude. An even bigger inconvenience results from the necessity to solve for the the inverse of a gradient in order to obtain $\overset{*}{\psi}$. Since the solution of these problems would be laborious and very time-consuming, it was decided to experiment with extrapolations of the stream-function. In particular, $\overset{*}{\psi}_{\ell}$ at the grid point ℓ was extrapolated directly from $\overset{*}{\psi}_i$ at the neighboring data points, as in the previous attempt:

$$\overset{*}{\psi}_{\ell} = \sum_{i=1}^{n} \gamma_i \overset{*}{\psi}_i \Big/ \sum_{i=1}^{n} \gamma_i . \qquad (5\text{-}3)$$

However, it was discontinued after the first trial because the number of areas of roughness increased. The only prospective way to solve this roughness in the field of $\overset{*}{\psi}$ is to use a more sophisticated objective analysis. Since such sophistication was beyond the scope of this study, the smoothing was simply performed by hand where needed.

Another problem, not directly related to the objective analysis, has to do with discontinuities in the flow pattern created by some mountains standing higher than the $\overset{*}{\psi}$ surface. Since the air either goes around or over these mountains, the very cumbersome operation of dealing numerically with the flow around irregular obstacles would have to be employed. In addition, the stability of the air mass would also have to be examined in order to determine what quantity of air most likely would tend to go over the top. Consequently, unless a complete barrier, such as a long mountain range existed, the streamlines were modified to show the probable deflections of the flow around the obstacle. A tentative but, perhaps, more realistic view of the passage of the air through and across the Canadian Cordillera in the lower levels of the atmosphere is thus obtained.

Due to the uncertainty of the decrease of terrain-induced vertical velocities with height, the estimates found in regions where the (smoothed) mountains are completely below the surface of $\overset{*}{\psi}$ cannot be justified. They appear generally too high, but the criterion used for the decrease of w with height may not be the only reason, for the grid length may also contribute to this discrepancy. In fact O'Neill(1966), while doing some work with a model for forecasting precipitation amounts, varied the grid length from three to one degree of latitude. He noticed that, as the grid length was decreasing, new centers of vertical velocities were appearing, and the magnitudes were increasing while the geographic location remained the same. Although the same problem may not apply here because of a different approach, similar results could be obtained with a change of grid length.

In order to explain the high values of orographic vertical

velocities being computed but not observed, McClain (1960) suggested that some of the air might stagnate along the mountains and, eventually, reduce the slope for the moving air above. However, it is felt that, even if the actual vertical velocities are only one-half to one-third of the values computed here, they are still highly significant.

Since the method used gives more weight to the winds, $\overset{*}{\psi}$ differs from Z if the wind is non-geostrophic, due to many factors such as friction and channelling, and the influence of observational, plotting, and transmission errors. In trying to minimize such effects, the weights in equation (3-10) were changed to 0.35, 0.35, and 0.3 respectively, but no significant modifications in the value of $\overset{*}{\psi}$ were observed. Such differences occurred in the central portion of the grid where the calculated wind velocities agreed fairly well with the winds reported at nearby data points, but the analysis of $\overset{*}{\psi}$ is somewhat smoother than that of Z.

In order to illustrate and partly circumvent these diverse problems, two maps[1] of the objective analysis are shown for each case. The first map in a set shows the results exactly as they are obtained from the objective analysis. The second map, a modified version of the first, shows what the analysis should probably look like when the influence of the high terrain on the flow is taken into account. Moreover, since the quantitative estimates of the terrain-induced vertical velocities should, perhaps, be considered simply as measures of order of magnitude, only the 2 cm/sec isotach of each center is shown on the second map.

---

[1] More details about the information on each map will be given in Chapter VI.

CHAPTER VI

PRESENTATION AND DISCUSSION OF RESULTS

Introduction

A total of five synoptic cases are studied in this investigation. Each case is represented by three maps. The first map in each set shows the original 850-mb analysis from which the data are abstracted. Contours are drawn at intervals of 200 geopotential feet. The second and third maps both illustrate the streamline and vertical velocity analyses discussed in Chapter V. Isopleths of $\overset{*}{\psi}$ are drawn every 30 gpm; vertical velocity isotachs are sketched at intervals of 2 cm/sec. The dashed lines on the first of the two objective analysis maps are the zero vertical velocity lines. The shaded areas represent mountains cutting through the $\overset{*}{\psi}$ surface. Such intersections are determined in the following way: With one geopotential meter very nearly equal to one geometric meter, all the grid points where

$$\overset{*}{\psi}(I, J) < H(I, J)$$

are simply enclosed by the locus of the common intersection. Since the surface $\overset{*}{\psi}$ is different for each synoptic situation, the shape of the obstacle intersection with $\overset{*}{\psi}$ varies somewhat from case to case. Streamlines carried through the high summits (indicated by dotted lines) show a discontinuity in the flow pattern and the air is assumed to surmount the obstacle in the calculations.

The objective analysis is bound to be different from the

subjective contour analysis because of the small grid length. Greater details are given and smoothing is more difficult. When comparing the objective analysis with the original contour analysis, it should be remembered that contours are not equivalent to, and do not in general coincide with a given set of streamlines.

A discussion[1] for each of the five synoptic cases analysed is given below.

1. SOUTHEASTERLY FLOW (FEBRUARY 9, 1958)

(a) Synoptic Situation (Figure (6-1))

The synoptic situation of February 9, 1958, is characterized by a low on the North Pacific, with a well-defined trough extending across the northwestern United States. A high pressure ridge extends from Alaska, across Alberta and Saskatchewan, and thence into the United States. A closed center of high has formed within this ridge along the Alberta-Saskatchewan border. A col is situated over the Yukon and the western part of the Northwest Territories. This synoptic pattern produces a generally southeasterly flow over much of the Canadian Cordillera.

(b) Objective Analysis (Figure (6-2))

The broad features of the synoptic pattern are readily discernible. However, the northern col is analysed differently by the objective method. Data are sparse in this region and it is difficult

---

[1] See Figures (6-17), (6-18) for the location of mountains, ranges, etc. referred to in the discussion.

to justify or give preference to either analysis. All that may be said is that the col is in the same general location on both analyses. The low in the Pacific is filled mainly because the estimated winds are not strong enough. The trough, the high center, and the ridge described earlier seem to be well located.

The problems discussed in Chapter V can be recognized in this case. Note the tight gradients in northeastern Saskatchewan, and along the Alaska-Yukon border near latitude 65°N. The same problem apparent at approximately latitude 55°N and longitude 140°W, is an example of the occurrence of roughness where it is felt that the estimates are based on sufficient data. The sharp ridge located to the south of the Mackenzie Mountains also seems to be a result of the same effect. Such roughness does not occur in the latter two regions in the other cases.

The sub-geostrophic winds have slackened the gradients in the Canadian Rockies. For example, contour 4400 gpf[1], corresponding to about 1350 gpm, is objectively analyzed to be more towards the ocean. The curvature in streamline 1410 agrees well with the direction of the reported wind at Prince George (XS). The slight meandering observed in streamline 1320 provides an example of the limit of smoothing allowable for a small grid length.

(c) Modified Objective Analysis (Figure (6-3))

On this map, the tight gradients and streamline 1320 have been smoothed. The sharp ridge near the Mackenzie Mountains has been rounded and somewhat shortened. The arrows near the obstacle boundary

---

[1] Geopotential feet.

intersections represent possible paths of the diverted flow. Streamline 1440 in Figure (6-2) is seen (by dotted lines) to come over the high mountains from which the Alberta Range emerges. In Figure (6-3), it is analysed along the east side of the Range to indicate that the air streams along the slopes. The dotted lines across the mountains mean to suggest now that some of the air may still flow over the top of ridges, in the manner indicated.

The division of streamline 1440 into two parts at the bottom left hand corner of the map implies that the air is diverted along the edges, especially to the north side. Streamline 1410 suggests that the air probably stays on the west side of the Alberta Range but goes to the east of the Stikine Mountains, with a small deviation to the west. At the same time, streamline 1380 suggests that the air flow remains to the west of the Coastal and Stikine Mountains although a small arrow indicates a slight deflection to the east of the Coastal Mountains. These streamlines show that very little air flows between these two obstacles.

Most of the air that crosses the mountains is flowing between the Coastal and Alberta Ranges, and then through a second gap between the Alberta Range and the Stikine Mountains. Further north, the air which has passed around the Stikine Mountains continues to blow along the coast with a major part going between the St. Elias and the Mackenzie Mountains before it streams over Alaska.

(d) Orographic Vertical Velocities (Figure (6-2))

A striking feature of the orographic vertical velocities is the strong area of ascent along the coast of the northwestern United

States where the flow is straight toward the mountains. The mountains are high in this area but the largest vertical velocities are associated with a hidden ridge extending northwestward from Eagle Peak (42°N, 120°W). This situation may seem unusual but it should be remembered that some higher values would certainly have been obtained at the points of discontinuity (shaded areas) if the computations had been carried out.

An area of strong ascent associated with the "concealed" Mount Baker is a dominant feature in north-central Washington where the air coming from a large basin is forced to rise over the mountain. This sudden rise is not followed by a strong descent on account of the manner intermountain valleys are handled by the computer program. Since the flow is mainly along the mountains over most of British Columbia, there are virtually no areas of extensive orographic lift. Weak forced ascents are produced over an area located north of Vancouver Island where a ridge extending from Mt. Waddington stretches across the flow, and in a second, relatively weak zone linked to the Stikine Mountains (see Figure (6-17)).

In northern Alberta, the dominant feature is the strong ascent associated with the Caribou Mountains, which is partly a result of the steep gradient developed in the objective analysis. Nevertheless, it remains an important singularity which appears also in other synoptic cases. Smaller areas of updraught and downdraught are generated also by the Swan Hills near Wagner (WA) which are, in this case, perpendicular to the flow.

An interesting feature in Alaska is the area of uplift associated with the hidden Mt. Marcus Baker. However, very little vertical motion is occurring between the St. Elias Mountains and Mt.

Blackburn, again an intermountain valley effect. The strong updraught north of Mt. Blackburn is induced by the Alaska Range just outside the grid. The larger vertical velocities over the Yukon are caused by strong gradients coupled with the steepness of the Mackenzie Mountains.

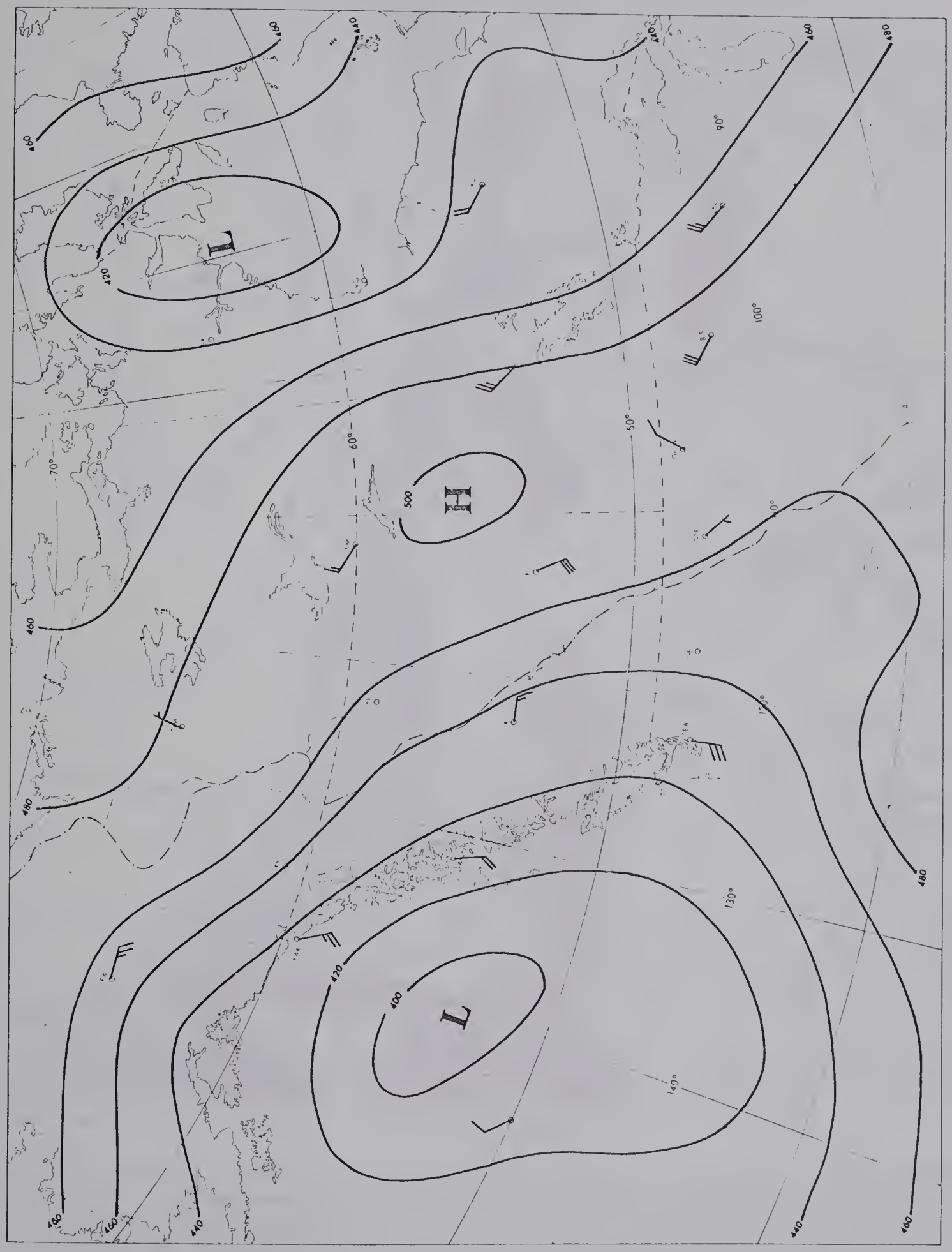

FIGURE (6-1) Original subjective analysis of the 850-mb surface for 00Z, February 9, 1958. The 200 gpf. contours are labelled in tens of feet.

FIGURE (6-2) Objective analysis of the 850-mb surface for 00Z, February 9, 1958. The stream-function ψ^* (heavy lines) is drawn at intervals of 30 gpm; and terrain-induced vertical velocity isotachs (thin lines), at intervals of 2 cm/sec. The broken lines represent zero vertical velocities. The letter A denotes ascending motion and D indicates centers of descending motion. Mountain complexes piercing the 850-mb surface are shaded in red.

FIGURE (6-3) Modified objective analysis of the 850-mb surface for 00Z, February 9, 1958. Modifications of the streamline analysis are indicated by arrows to show the deflections around high obstacles. Areas of orographically induced vertical motion are outlined by the 2 cm/sec isotach. The letters A and D represent ascending and descending motion.

2. NORTHWESTERLY FLOW (MARCH 4, 1958)

(a) Synoptic Situation (Figure (6-4))

The synoptic situation of March 4, 1958 presents two well-defined ridges across northern British Columbia and northwestern United States, both offshoots of a Pacific high centered just to the south of the weather ship Papa (4YP). A weak trough is lying over Coppermine (CO), while a second, better developed trough, extends across Hudson Bay, the Prairie provinces, and south of Great Falls (GTF) where it is somewhat accentuated as shown by contour 4800 gpf. A generally northwesterly flow is thus generated over the principal region.

(b) Objective Analysis (Figure (6-5))

The objective analysis was able to reproduce most of the broad features referred to in the previous section. The high center over the Pacific is well located with the same central intensity. The two ridges across northern British Columbia and the northwestern United States are still distinguishable but less prominent. The troughs over the Prairies and near Coppermine are placed much as on the contour map.

The pattern configuration over the Gulf of Alaska shows up well except that the ridge over Alaska is accentuated and more strongly curved. This is presumably caused by the grouping of the streamlines in the northern critical area near the Yukon Alaska border. The cyclonic curvature shown by streamline 1500/4900[1] east of Yakutat (YAK)

---

[1] Streamlines and contours will be labelled in gpm and gpf when it is thought to be helpful for ready comparison and conversion.

would be more evident on the original subjective analysis if contour 4900 were analyzed. A trough definitely exists between the two ridges bounding this region. The gradient is weakened near Fort Nelson (YE) where the contour 4800/1470 is now located further west on the objective analysis, while contour 4600/1410 remains nearly in the same position.

(c) Modified Objective Analysis (Figure (6-6))

The only major barrier to this circulation is the high terrain in the northwestern United States. As in the southeasterly synoptic situation, the flow is essentially along the major mountain chains. The only passage of air into Alberta exists between the Mackenzie and the Stikine Mountains. Relatively little air flows between the Stikines and the Alberta Range: the major unimpeded channels are along the western slopes of Alberta.

A separation of the flow, mostly to the east of the Stikine Mountains, is shown by streamline 1470, while streamline 1410, which crosses part of the Mackenzie Mountains, suggests that the air currents will tend to follow the western slopes. Streamline 1500 represents the air flowing to the west of the St. Elias Mountains but part of the stream may also be running to the east side; this branching is not indicated in the figure. However, a definite separation of the flow is shown around the Coastal Mountains in southern British Columia, followed by an amalgamation of the two branches over the lower terrain in Washington State.

(d) Orographic Vertical Velocities (Figure (6-5))

The vertical motion pattern is similar to the southeasterly synoptic situation, but with the difference that the centers of updraught and downdraught are interchanged. The weak circulation over Alberta produces only slight orographic effects; no marked centers are associated with the Caribou Mountains.

Certain characteristics of this vertical motion field deserve to be specified. The area upwind from the Coastal Mountains displays an elongated tongue of ascending air linked with a narrow ridge extending along the flow from Mt. Waddington. The air climbs gradually along this ridge but there may well be some branching around the higher peaks.

Compared to the southeasterly case, a broader area of ascent is associated with the Stikine Mountains. In fact, the shape of the 4000 foot contour in Figure (4-6) indicates that the mountain offers a broader and steeper barrier to the northwesterly flow than to the flow from the southeast.

Over the Yukon, a probably excessive amount of forced lift is associated with a long ridge of the Mackenzie Mountains.

FIGURE (6-4) Original subjective analysis of the 850-mb surface for 00Z, March 4, 1958. The 200 gpf. contours are labelled in tens of feet.

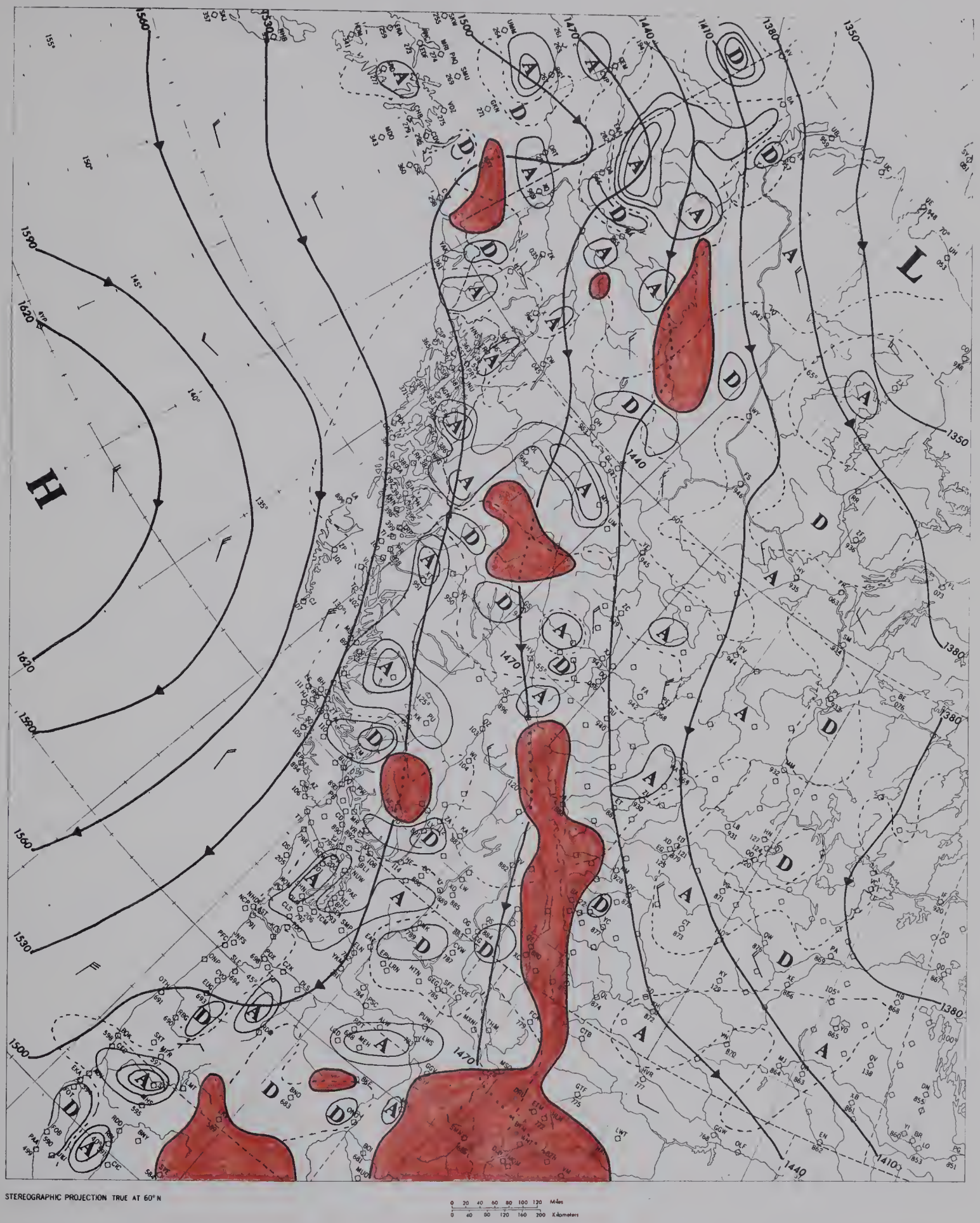

FIGURE (6-5) Objective analysis of the 850-mb surface for 00Z, March 4, 1958. The stream-function ψ^* (heavy lines) is drawn at intervals of 30 gpm; and terrain-induced vertical velocity isotachs (thin lines), at intervals of 2 cm/sec. The broken lines represent zero vertical velocities. The letter A denotes ascending motion and D indicates centers of descending motion. Mountain complexes piercing the 850-mb surface are shaded in red.

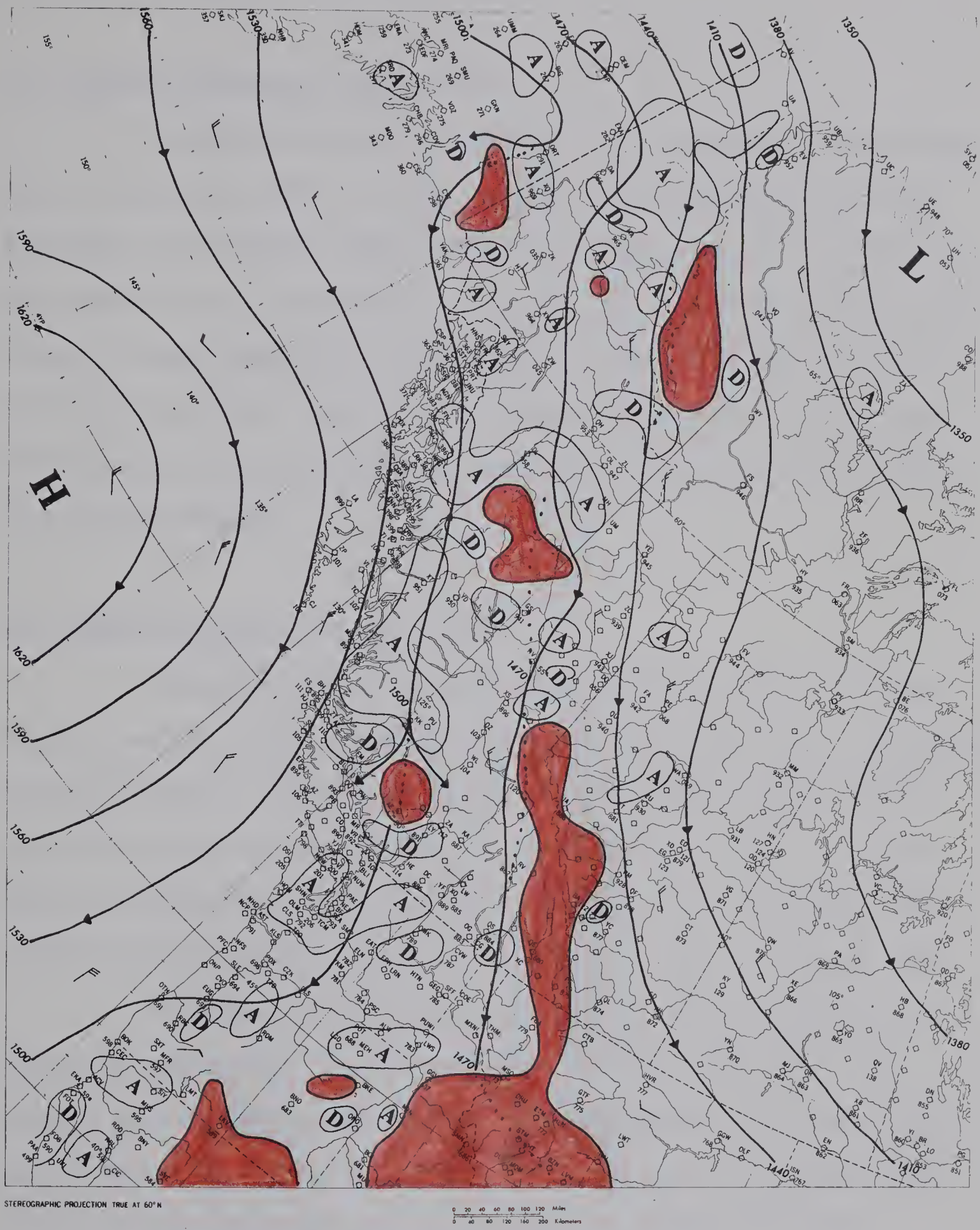

FIGURE (6-6) Modified objective analysis of the 850-mb surface for 00Z, March 4, 1958. Modifications of the streamline analysis are indicated by arrows to show the deflections around high obstacles. Areas of orographically induced vertical motion are outlined by the 2 cm/sec isotach. The letters A and D represent ascending and descending motion.

3. SOUTHWESTERLY FLOW (JANUARY 17, 1958)

(a) Synoptic Situation (Figure (6-7))

An important case of orographic flow is depicted on the 850-mb map of January 17, 1958. A well-defined trough associated with a low centered east of Kodiak (NHB) extends east-southeastward across Alberta and Saskatchewan. An anticyclone with a ridge stretching northeastward towards Glasgow (GGW) and Bismark (BIS) is established over the northwestern U.S., while a smaller closed high is centered over Hudson Bay. This synoptic situation produces a generally southwesterly flow across the Canadian Rockies.

(b) Objective Analysis (Figure (6-8))

The southwesterly circulation is maintained over most of the region, and the trough extending from Alaska into Alberta and Saskatchewan is well located. However, the objective analysis does not correlate so well in the Northwest Territories, where the ridge over Great Bear Lake is modified drastically by the bunching of the streamlines. Some lesser differences exist also over Yukon, e.g., along streamline 1290.

The behavior of streamline 1470/4800 over Saskatchewan requires an explanation. As in the previous southeasterly case, its changed orientation results from a different analysis of the col shown on the 850-mb map to the southwest of Lake Winnipeg. The marked bend in the ridge over Saskatchewan is probably an exaggeration and a doubtful feature, because it is so close to the critical area in the northeastern part of Saskatchewan.

(c) Modified Objective Analysis (Figure (6-9))

The main passageway for the air at the 850-mb level to reach Alberta is between the Stikine Mountains and the Alberta Range. A second passage between the Mackenzie and Stikine Mountains admits the flow into the upper Mackenzie Basin. Yet a third passage between the St. Elias and Mackenzie Mountains allows the air to penetrate into the Yukon.

The separation of the flow around Mt. Good Hope (see streamline 1440) suggests that a small amount of air flows past this mountain complex toward the Alberta Range. Streamline 1530 near the bottom left hand corner shows the deflection of the air towards the north; however, some of the flow is probably stalled and deflected southwestward along the coast.

The shape of the Stikine Mountains in this particular situation is favorable for a convergence of the flow in the valley facing west. Although a similar valley exists in the Mackenzie Mountains, the influx of air is largely blocked by the southern ridge.

(d) Orographic Vertical Velocities (Figure (6-8))

The isotachs of forced vertical motion reflect the fact that a southwesterly flow is nearly perpendicular to the mountains. The West Coast between latitude 40°N to 60°N is a region of ascent with the larger speeds associated with the high peaks. The grouping of the isotachs in the valley of the Stikine Mountains discussed earlier, clearly marks an important zone of convergence.

The main area of subsidence is concentrated along the lee of the Alberta Range. Lethbridge (QL) enclosed by the 2 cm/sec isotach,

reports a high surface temperature of 49°F, whereas other stations further to the east of the Divide such as Medicine Hat (XH) with 42°F, and Swift Current (YN) with 33°F, show a decrease in temperature even though all three stations were analyzed to be in the same air mass.

An interesting feature in the field of vertical motion is a closed center (which is not labelled) located just to the west of Seattle (SEA). This closed isoline is a positive 2 cm/sec isotach and not a 6 cm/sec isotach as it may appear, because it is practically enclosed by a 4 cm/sec line. This involves grid point (72, 33), (see Figure (4-6)) which has a lower height than any of the four other points involved in computation of w[1]; hence, the criterion for intermountain valley applies. A quick calculation shows that the slope is negative along the abscissa of the grid, and positive along the ordinate with twice the magnitude of the former. The geostrophic wind velocity at grid point (72, 33) being generally 18 knots from the west, subsidence should occur since the v-component is much less than the u-component. Indeed, the value computed by equation (4-21) is -0.07 cm/sec. The feature is a perfect example of a small dip of the air over a valley, as discussed in Chapter IV.

The light to moderate orographic lift over the Great Bear Lake region is largely the result of the high wind speeds generated by the roughness of the field; consequently, they are not reproduced on the modified objective analysis (Figure (6-9)).

---

[1] See Appendix A and Figure (4-3)

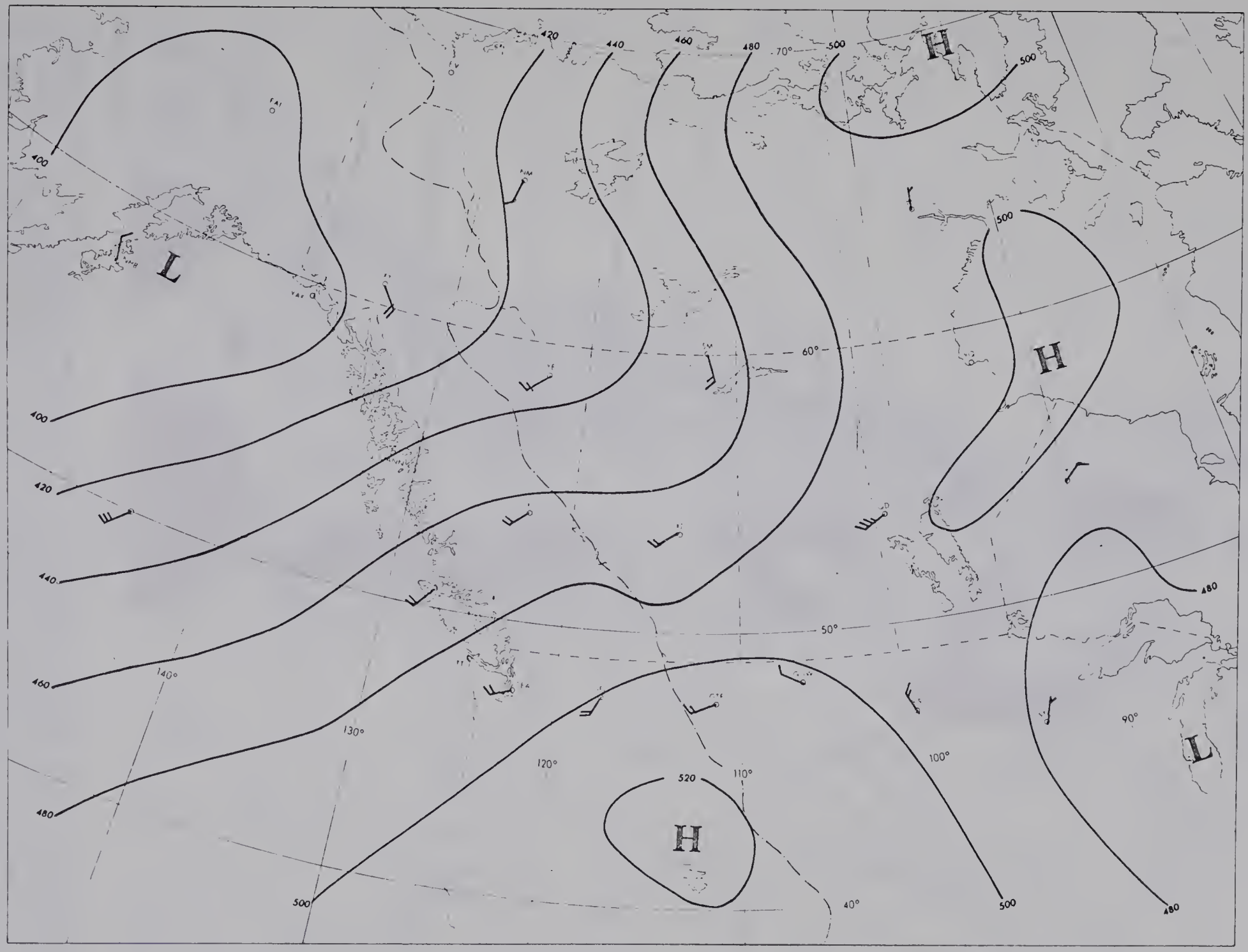

FIGURE (6-7) Original subjective analysis of the 850-mb surface for 00Z, January 17, 1958. The 200 gpf. contours are labelled in tens of feet.

FIGURE (6-8) Objective analysis of the 850-mb surface for 00Z, January 17, 1958. The stream-function ψ^* (heavy lines) is drawn at intervals of 30 gpm; and terrain-induced vertical velocity isotachs (thin lines), at intervals of 2 cm/sec. The broken lines represent zero vertical velocities. The letter A denotes ascending motion and D indicates centers of descending motion. Mountain complexes piercing the 850-mb surface are shaded in red.

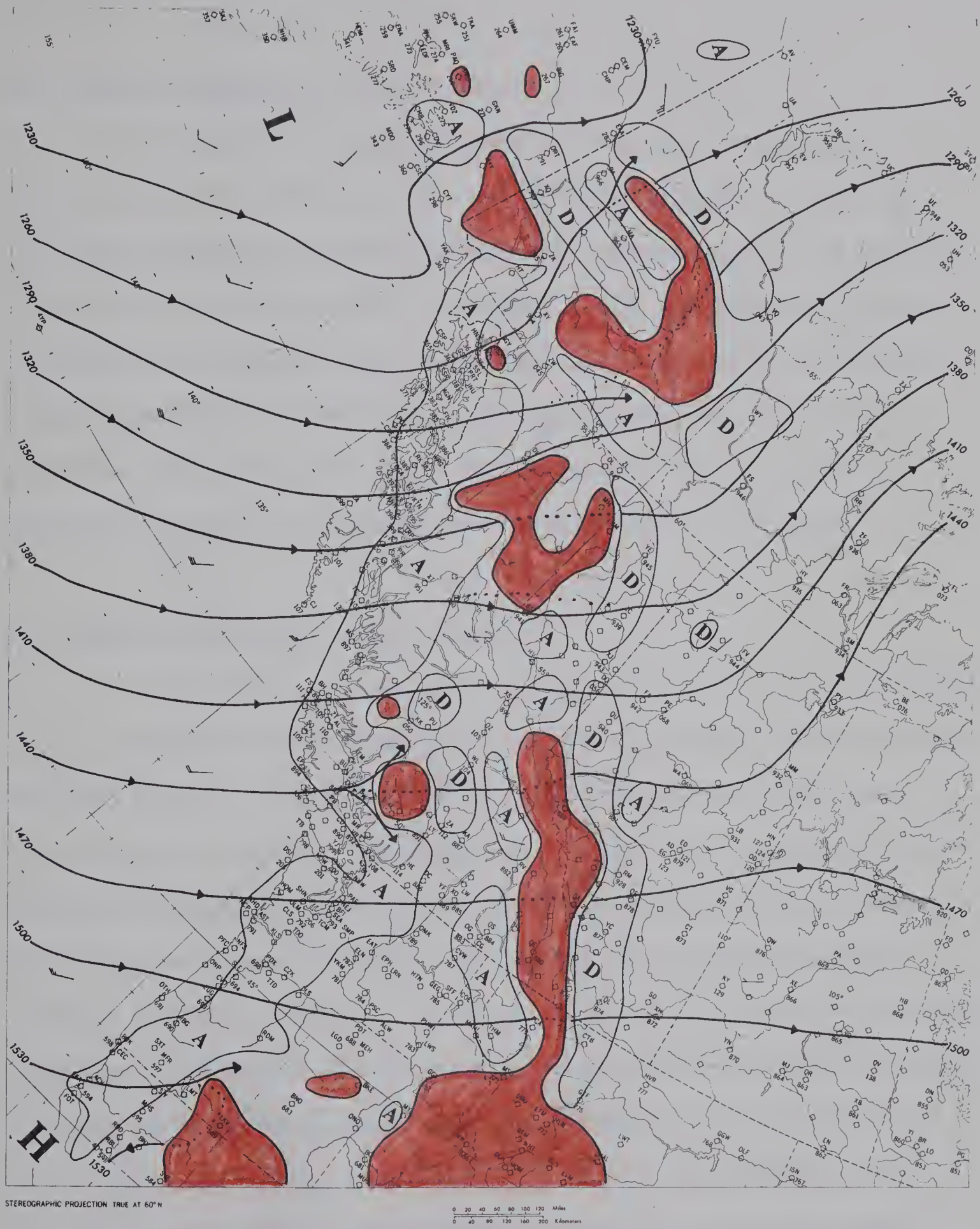

FIGURE (6-9) Modified objective analysis of the 850-mb surface for 00Z, January 17, 1958. Modifications of the streamline analysis are indicated by arrows to show the deflections around high obstacles. Areas of orographically induced vertical motion are outlined by the 2 cm/sec isotach. The letters A and D represent ascending and descending motion.

4. WESTERLY FLOW (JANUARY 4, 1958)

(a) Synoptic Situation Figure (6-10))

An example of synoptic-scale westerly flow is shown in Figure (6-10), the 850-mb contour map for 12Z, January 4, 1958. A cyclonic system and associated trough which extends across the Prairies, covers most of the Yukon and a good part of the Northwest Territories. An anticyclone centered south of Spokane (GEG), with a well-developed ridge projecting northwestward across the Pacific and into Alaska, dominates the northwestern U.S. This synoptic situation produces a generally westerly circulation over the four western provinces.

(b) Objective Analysis (Figure (6-11))

The large scale features are reproduced well, except apparently in the Great Slave-Great Bear Lake area where, at first glance, the two analyses appear to disagree; however, closer inspection shows that they are quite similar. The objective analysis does not extend streamline 1230/4000 as far east as the subjective analysis does. It cuts the trough to the west of Norman Wells (VQ) in accordance with the reported southerly wind, but the basic nature of the flow pattern remains unchanged. Because of the orientation of the grid, streamline 1260/4100 is shown to be in three segments which might create some confusion at first sight. The ridge over Inuvik (EV) is the only doubtful feature, but its presence could be justified as being part of the same Arctic high which ridges southward over Coppermine (CO).

The Pacific ridge is clearly evident, although it is somewhat disturbed west of Vancouver Island by a small trough in streamline

1470, a feature most likely introduced by a lack of data. No evidence of such a trough exists in the original analysis. The trough over the Prairies is reproduced correctly but it is somewhat over-emphasized by the grouping of the streamlines in northeastern Saskatchewan.

(c) Modified Objective Analysis (Figure (6-12))

Most of the air has to surmount the Alberta Range, in this case the major obstacle to the flow; very little air is deflected southward. The Mackenzie Mountains present another large obstruction to the circulation. Moreover, the air is now streaming directly into the valley referred to in the previous case. This circulation has the same two passages open for air streaming to Alberta as the flow from the southwest with the exception that both channels now appear to be of equal importance.

Only a small amount of air flows between Mt. Good Hope and the Alberta Range, as shown by streamline 1500. Both streamlines 1350 and 1380 illustrate the separation of the air flow towards the two passages at the Stikine Mountains. The same situation occurs at Mt. Waddington and the northern edge of the Alberta Range (see streamline 1470).

(d) Orographic Vertical Velocities (Figure (6-11))

With a reasonably weak circulation over northwestern U.S., very little orographic lift is apparent. As in the southwesterly situation, very strong uplift takes place along the coast of British Columbia. Relatively little subsidence occurs east of the Coastal Mountains but the major downdraft happens along the eastern flank of the Rockies from the Mackenzie Mountains to Lethbridge (QL).

The strong subsidence in southwestern Alberta suggests the presence of a Chinook. Figure (6-13) shows part of the surface weather reports at some stations on both sides of the Continental Divide for the particular time. Because Kimberley and Lethbridge are at about the same elevation, the 25°F temperature change between them is much too large to be accounted for in terms of elevation differences. Both Lethbridge and Calgary have westerly winds and large temperature-dew point spreads ($T - T_d$). Further north a strong updraught is associated with the Caribou Mountains.

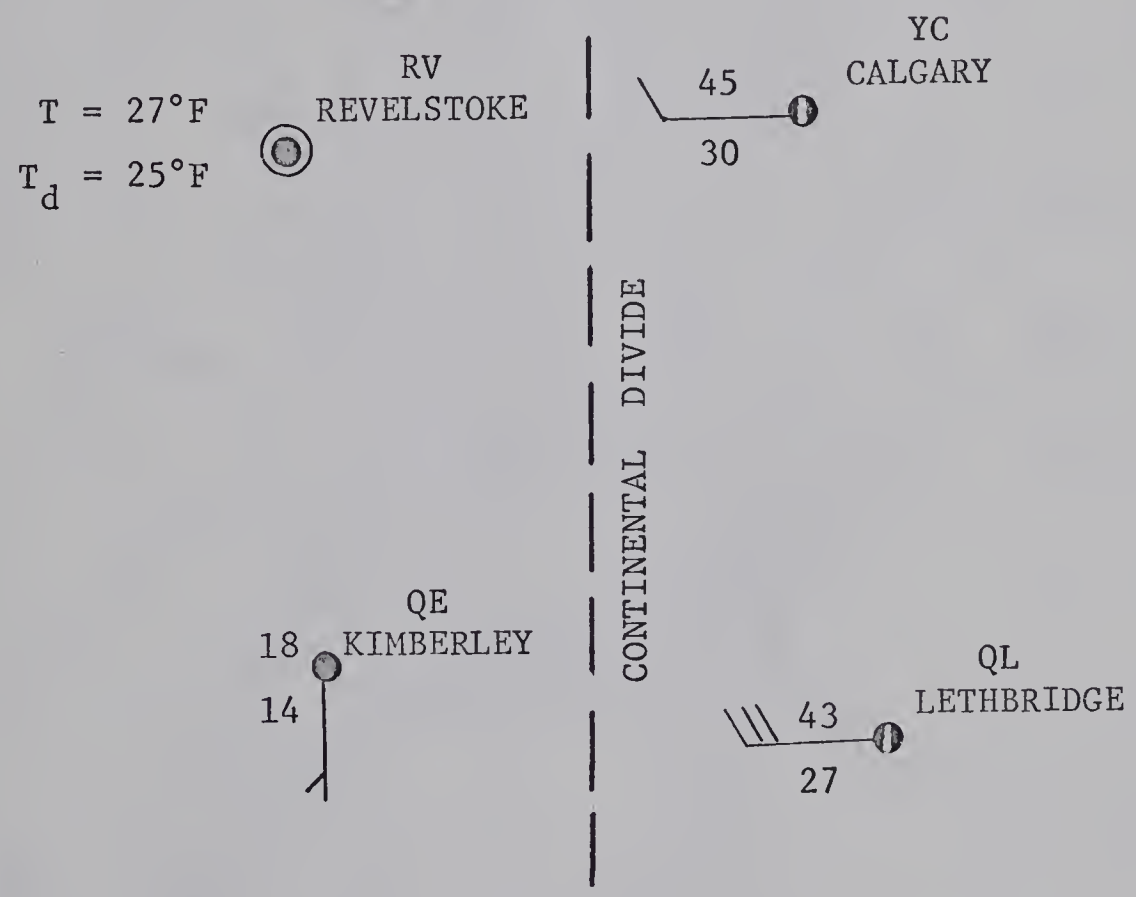

FIGURE (6-13) Temperatures, dew points, cloud cover and winds at four stations on opposite sides of the Continental Divide.

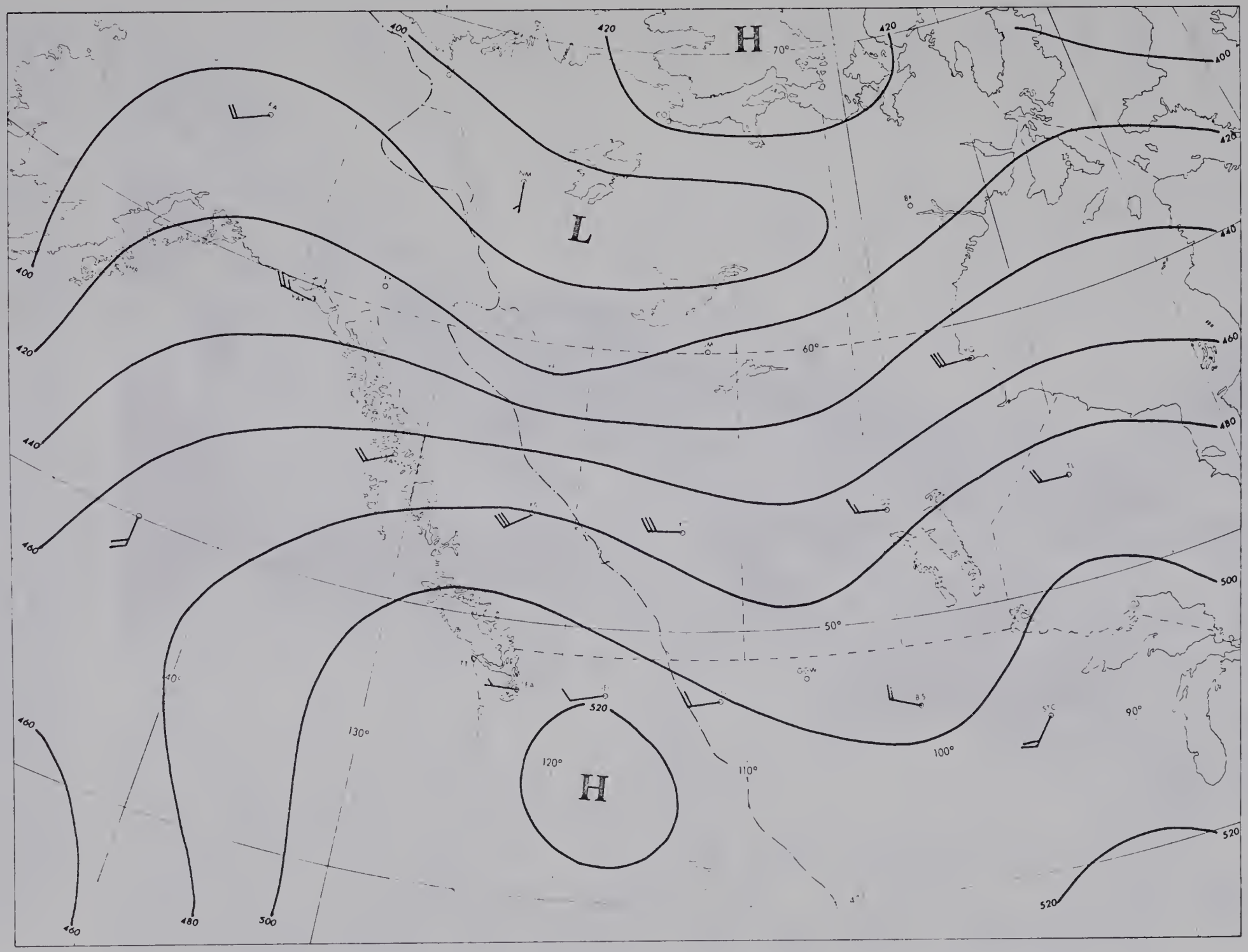

FIGURE (6-10) Original subjective analysis of the 850-mb surface for 12Z, January 4, 1958. The 200 gpf. contours are labelled in tens of feet.

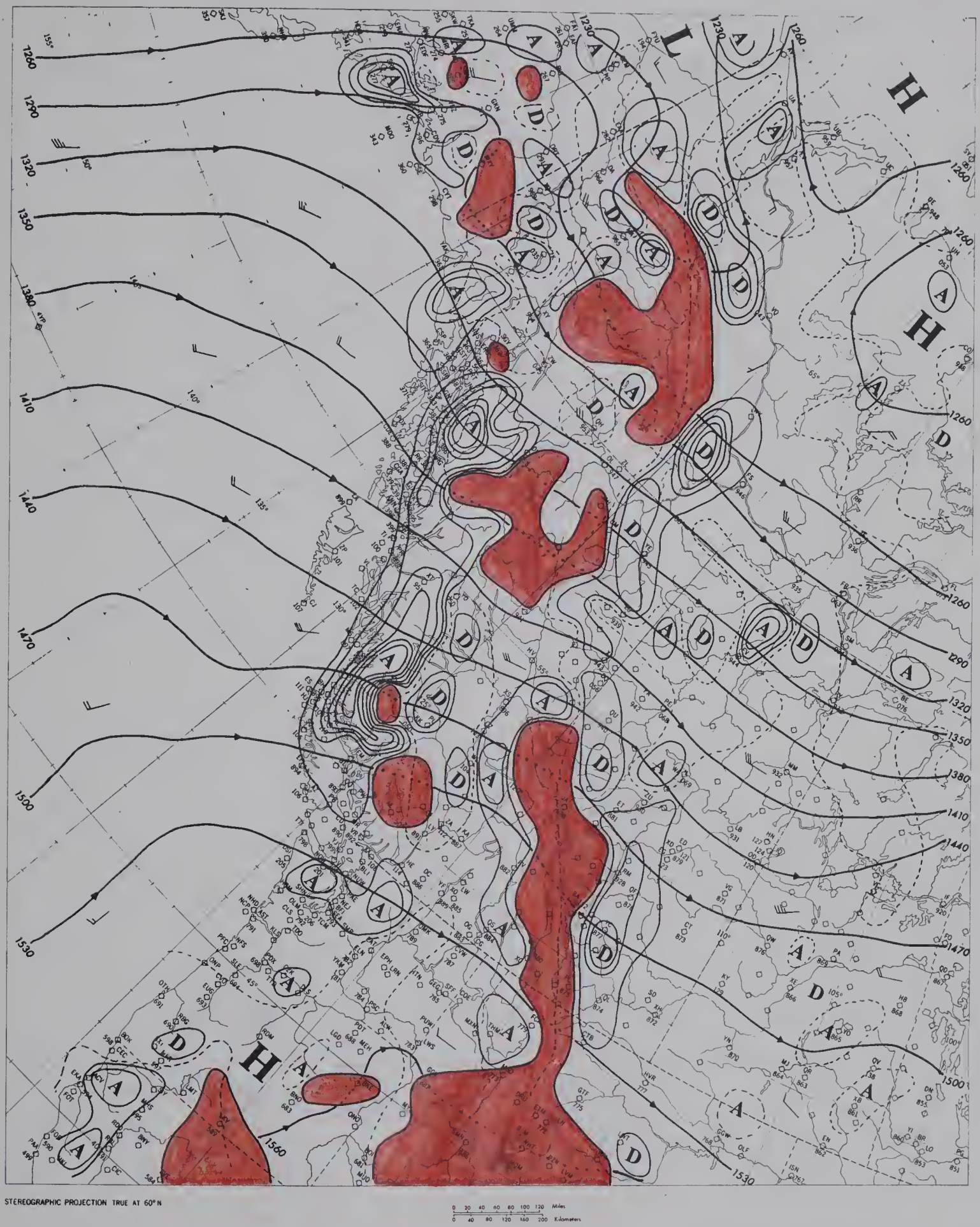

FIGURE (6-11) Objective analysis of the 850-mb surface for 12Z, January 4, 1958. The stream-function ψ^* (heavy lines) is drawn at intervals of 30 gpm; and terrain-induced vertical velocity isotachs (thin lines), at intervals of 2 cm/sec. The broken lines represent zero vertical velocities. The letter A denotes ascending motion and D indicates centers of descending motion. Mountain complexes piercing the 850-mb surface are shaded in red.

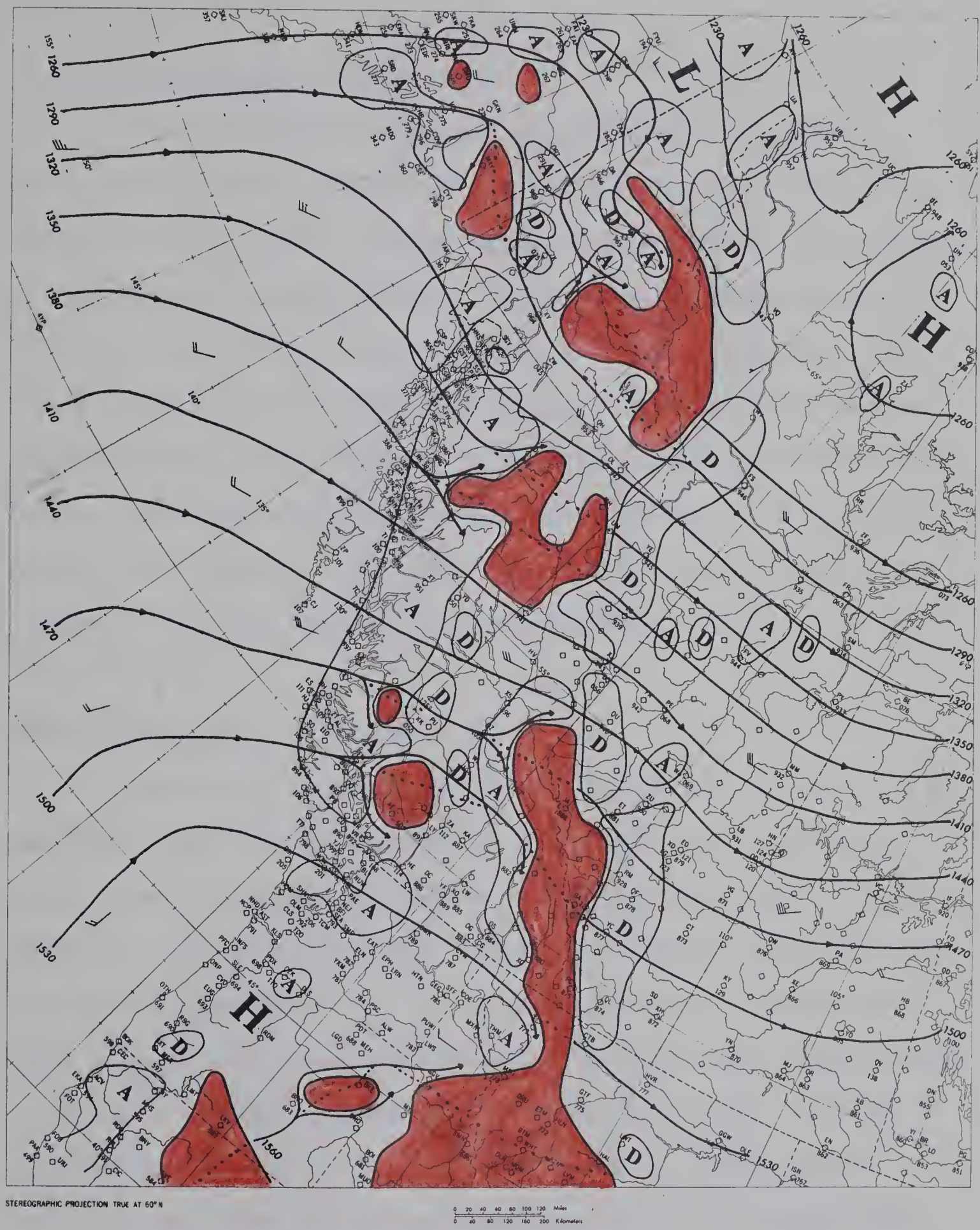

FIGURE (6-12) Modified objective analysis of the 850-mb surface for 12Z, January 4, 1958. Modifications of the streamline analysis are indicated by arrows to show the deflections around high obstacles. Areas of orographically induced vertical motion are outlined by the 2 cm/sec isotach. The letters A and D represent ascending and descending motion.

5. EASTERLY FLOW (MARCH 6, 1958)

(a) Synoptic Situation (Figure (6-14))

The synoptically important easterly circulation pattern, the "upslope" case for Western Alberta, is shown on the 850-mb map for 00Z, March 6, 1958. A trough extends southward from a low centered in southeastern British Columbia. Another trough extends eastward along latitude 60°N from a depression located over Alaska. Yet another trough covers most of the Northwest Territories while a small low is centered south of Lake Winnipeg. A broad ridge is established over the Pacific and a weak high has developed over the Yukon. A col is thus formed in the vicinity of Annette (ANN) . This synoptic situation produces an easterly flow over the southern half of Alberta and B.C.

(b) Objective Analysis (Figure (6-15))

Excepting the few extra meanders in the two main sections of streamline 1410, and the bunching of the streamlines in northeastern Saskatchewan, the objective analysis has performed very well. The depression over southern British Columbia is reproduced with the same shape and central intensity. The sharp trough south of Spokane and Great Falls in the contour 4400 has been flattened, but streamline 1380 maintains it in the right position. The col near Annette (ANN) is analyzed differently, as in all previous cases involving similar patterns. The small anticyclone located south of The Pas (QD) does not appear on the subjective 850-mb analysis, but the existence of a small centre of high is supported by the anticyclonic wind circulation which appears on the original weather office chart.

(c) Modified Objective Analysis (Figure (6-16))

As in the westerly flow, the major barriers to the circulation are the Alberta Range and the high mountains of the northwestern U.S. However, because of the location of the depression, the air has to surmount the Range in opposite directions; toward the west in the northern section, and toward the east in the southern section. Most of the air remains north of the high terrain in northwestern U.S. as indicated by streamline 1380.

The orientations of streamline 1380 around the northern edge of the Alberta Range, of streamline 1350 around the Coastal Mountains, and of streamline 1410 around the Stikine Mountains indicate a deflection of the air current towards the major passage of the air to the coast between the Stikine and Coastal Mountains. An intermediate streamline 1395 is added to indicate that the flow probably separates at the St. Elias Mountains.

(d) Orographic Vertical Velocities (Figure (6-15))

This synoptic situation produces relatively weak orographic effects. With an easterly flow at the Alberta Range, a gradual ascent, rather than a sudden rise when an onshore flow prevails along the coast of British Columbia, is indicated by the lesser intensity of the isotach centers. Nevertheless, this slow pattern of ascent is of considerable meteorological importance in that prolonged motion of moist air from the east or northeast will lead to widespread "upslope" conditions of low cloud and drizzle in much of Alberta.

North of the Stikine Mountains the air flows along the mountain chains as in a southeasterly flow. However, only weak orographic effects

are produced over northwestern B.C. and the Alaskan Panhandle on account of the weak circulation in the col. Some subsidence occurs along the B.C. coast. The major area is located west of the ridge (discussed in the northwesterly case) extending northwestward from Mt. Waddington. The largest values prevail to the north of Vancouver Island because farther south the high terrain of the Island creates an intermountain valley with the Coastal Mountains.

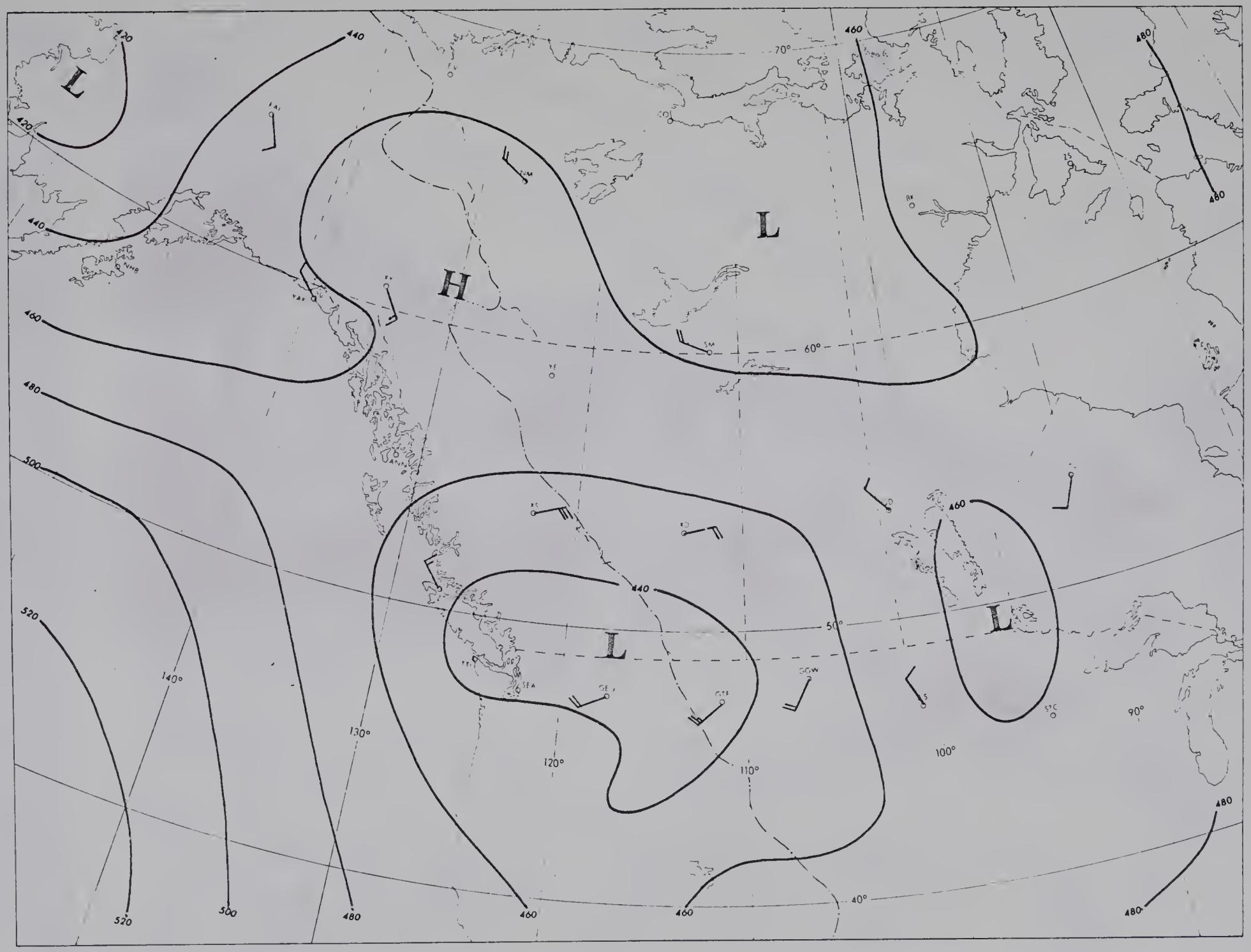

FIGURE (6-14) Original subjective analysis of the 850-mb surface for 00Z, March 6, 1958. The 200 gpf. contours are labelled in tens of feet.

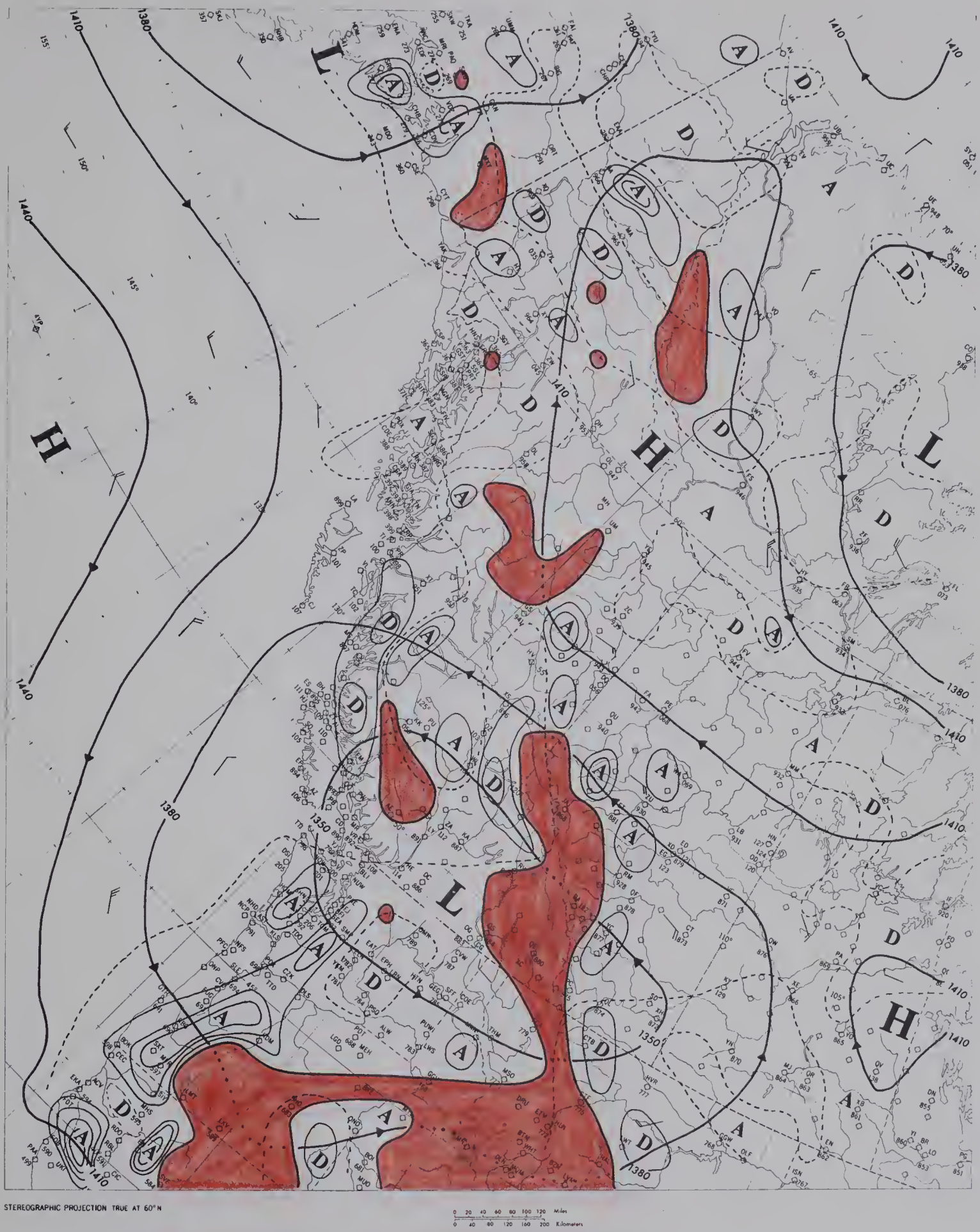

FIGURE (6-15) Objective analysis of the 850-mb surface for 00Z, March 6, 1958. The stream-function ψ^* (heavy lines) is drawn at intervals of 30 gpm; and terrain-induced vertical velocity isotachs (thin lines), at intervals of 2 cm/sec. The broken lines represent zero vertical velocities. The letter A denotes ascending motion and D indicates centers of descending motion. Mountain complexes piercing the 850-mb surface are shaded in red.

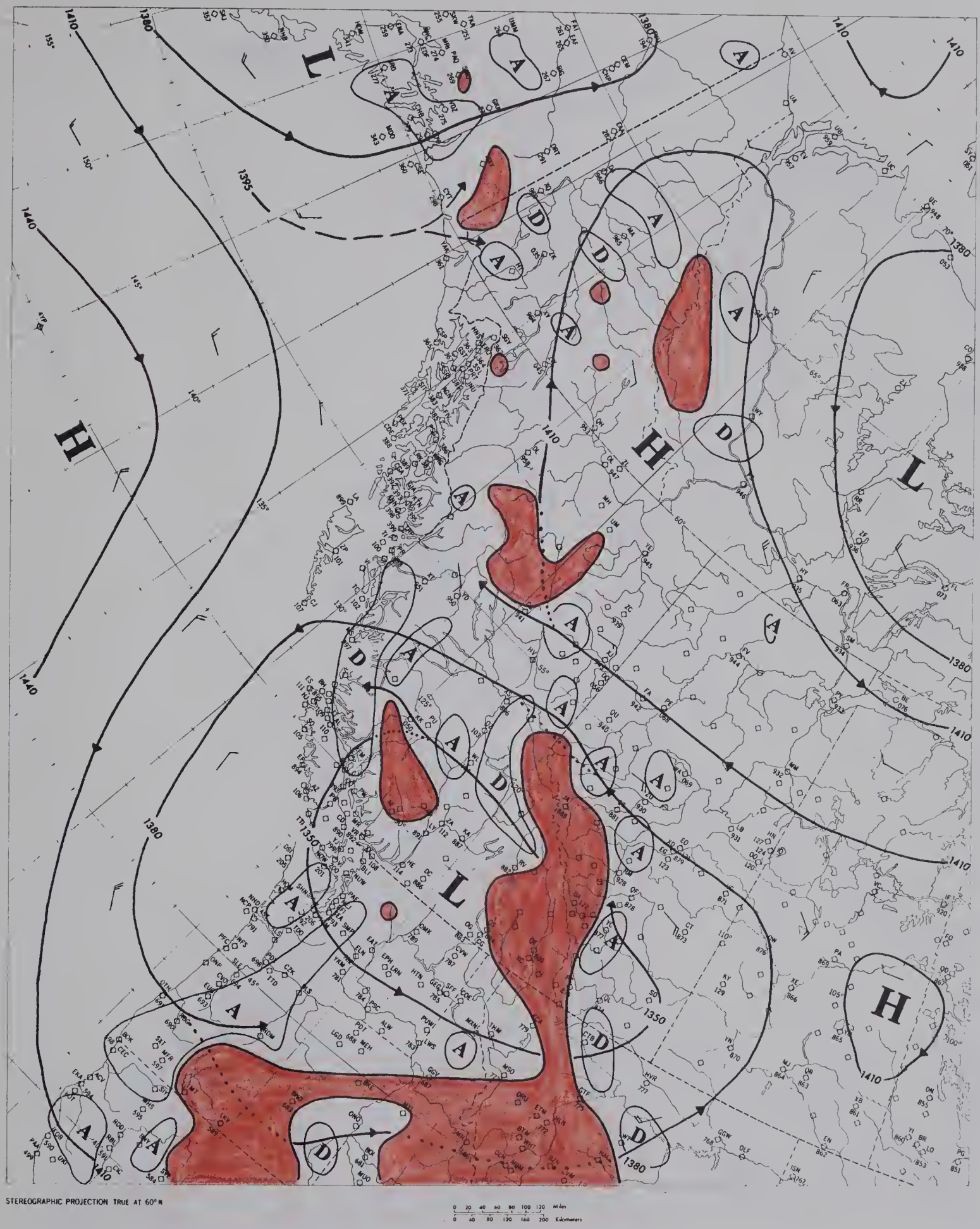

FIGURE (6-16) Modified objective analysis of the 850-mb surface for 00Z, March 6, 1958. Modifications of the streamline analysis are indicated by arrows to show the deflections around high obstacles. Areas of orographically induced vertical motion are outlined by the 2 cm/sec isotach. The letters A and D represent ascending and descending motion.

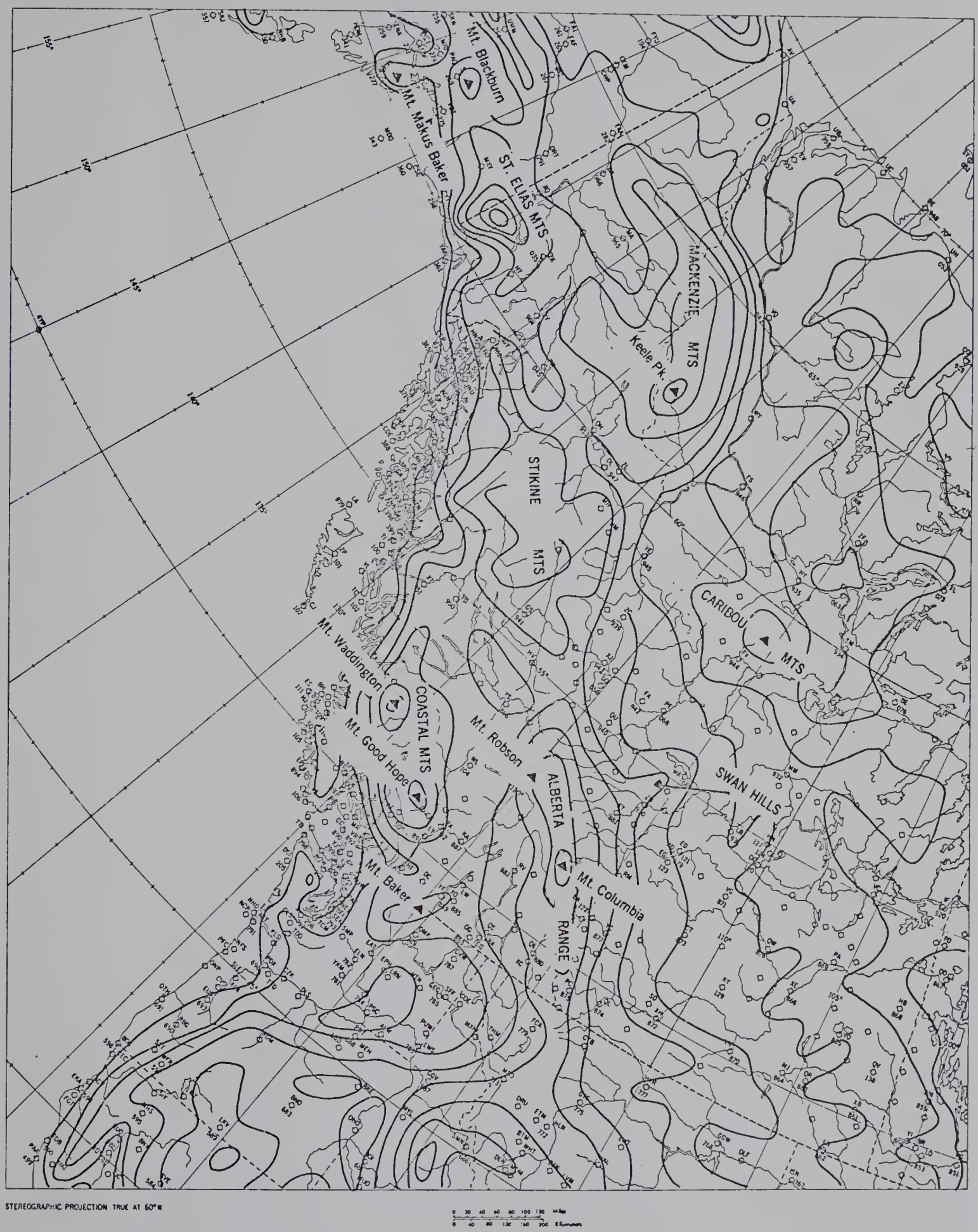

FIGURE (6-17) The same smoothed height profile as Figure (4-6) but with the names of significant peaks and mountain chains included.

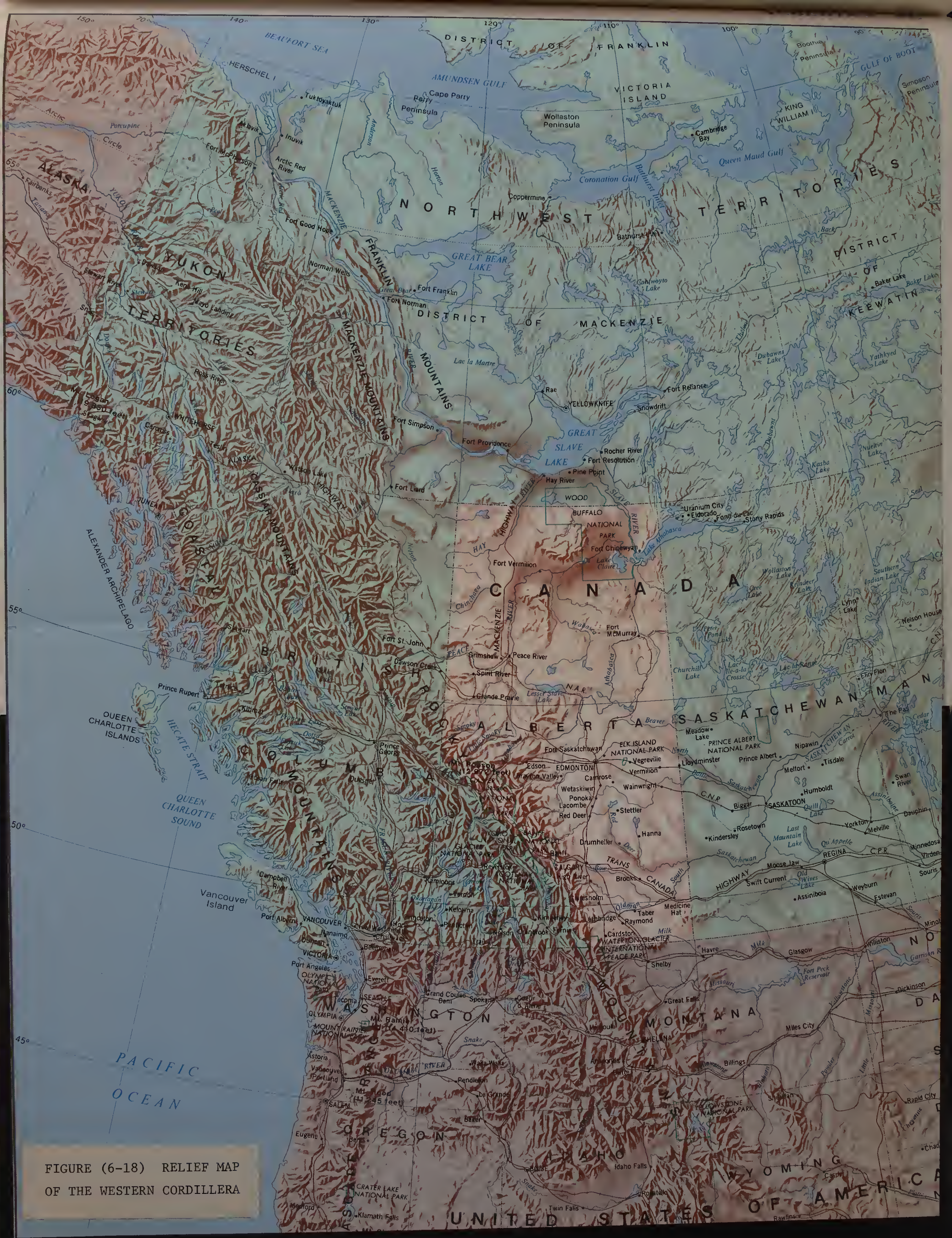

FIGURE (6-18) RELIEF MAP OF THE WESTERN CORDILLERA

CHAPTER VII

CONCLUSIONS AND SUGGESTIONS FOR FURTHER WORK

Conclusions

The procedures employed in this study, as in any similar analysis, are amenable to various refinements in terrain and finite-difference smoothing. Even though the approach taken here is simple and not above criticism on a number of points, the objective analysis has, on the whole, well served the purpose of this investigation.

This study examines the effect of mountain barriers on the 850-mb flow of five typical synoptic situations of Western Canada. The complexity of the flow in the Canadian Rockies in the lower levels of the atmosphere is outlined in considerable detail and the major passages of air around and between the obstructions of high terrain are indicated in each case. This is of some practical importance because operational meteorologists often neglect to consider the presence of the mountains when they analyze contours and isotherms at low levels such as at the 850-mb surface.

Although the magnitudes of the vertical motion vectors may appear too large, actual vertical velocities may be locally even higher since they would be generated by the actual, unsmoothed height profile. The values obtained depend very much on the criterion used for the decrease of the vertical components with height and on the assumption that the air surmounts the obstacle. Nevertheless, the analyses show the areas of potential ascent and descent which may not be apparent or

realized in these mountainous regions. More generally, the analysis of streamlines in regions which may, on casual inspection, seem free of orographic effects frequently reveals some ridge or other topographic feature that will, under certain conditions, impede and modify the flow significantly.

Since weather offices now have access to on-line computers, improved objective analyses that do not require too much computer time could be used operationally to estimate orographic vertical velocities, and alert the forecasters to possible developments resulting from terrain influences. It is to be expected that more sophisticated approaches to the problem of orographic flow in the Canadian Cordillera will bring out, in due course, other interesting and operationally significant features.

Suggestions for Further Work

The objective analysis used in this study will certainly have to be improved to accommodate a smaller grid length. In addition, it should be able to deal with actual winds in the mountainous regions. However, such information is usually not available at present in remote areas, and further advances will probably have to await the establishment of a better observational network.

Estimates of the orographic vertical velocities could be calculated also at a higher level such as at the 700-mb surface which would be entirely above the smoothed profile. A more sophisticated model involving polynomials to estimate the heights at grid points could probably be made to work with fewer station-observed input data, but, perhaps the newer satellite systems capable of the remote sensing

of atmospheric temperature and humidity will circumvent the problem of inadequate data input in the near future.

The decrease of the vertical velocities with height, mentioned in Chapter IV, will have to be examined further if more realistic magnitudes are to be obtained. Thus, it might be desirable to reduce geostrophic wind speeds in inverse proportion to the distance of the pressure surface from the ground. Friction would then be taken into account as well. Furthermore, the grid length should be varied to check O'Neill's results about the magnitudes increasing with decreasing grid length. If such a variation exists, it will be necessary to determine which mesh size is best suitable. Once a realistic pattern has been obtained, by whatever procedure, it would be interesting to relate the results to cloud cover and precipitation.

BIBLIOGRAPHY

Agnew, T., 1969: Terrain-induced vertical velocities obtained using a direct method of stream-function computation, Technical Memoranda, Department of Transport, Meteorological Branch, No. 721, 26 pp.

Atkins, M., 1970: Objective analysis of upper air height and humidity data on a fine mesh, Meteor. Mag., 49, 98-110.

Bjerkness, J. and H. Solberg, 1921: Meteorological conditions for the formation of rain, Geofys. Publikasjoner, 2, No. 3, 1-60.

Bonacina, L., 1945: Orographic rainfall and its place in the hydrology of the globe, Quart. J. Roy. Meteor. Soc., 71, 41-55.

Bushby, F. and V. Huckle, 1957: Objective analysis in numerical forecasting, Quart. J. Roy. Meteor. Soc., 83, 232-247.

_____, and M. Timpson, 1967: A 10-level atmospheric model and frontal rain, Quart. J. Roy. Meteor. Soc., 93, 1-17.

Butler, R. and E. Kerr, 1962: An Introduction to Numerical Methods, Sir Isaac Pitman and Sons Ltd., London, 386 pp.

Cook, A. and A. Topil: Some examples of chinooks east of the mountains of Colorado, Bull. Amer. Meteor. Soc., 33, 42-47.

Cressman, G., 1959: An operational objective analysis system, Mon. Wea. Rev., 87, 367-374.

Douglas, C. and J. Glasspoole, 1947: Meteorological conditions in heavy orographic rainfall in the British Isles, Quart. J. Roy. Meteor. Soc., 73, 11-42.

Elliott, R. and R. Shaffer, 1962: The development of quantitative relationships between orographic precipitation and air-mass parameters for use in forecasting and cloud-seeding evaluation, J. Appl. Meteor., 1, 218-228.

Endlich, R. and R. Mancuso, 1964: A direct method of stream-function computation, Tellus, 16, 32-39.

_____, and R. Mancuso, 1965: Objective Analysis and Forecasting of Clear Air Turbulence, Stanford Research Institute, Menlo Park, California, Contract CWb-10871, 56 pp.

Estoque, M., 1957: A graphical integrable prediction model incorporating orographic influence, J. Meteor., 14, 293-296.

Gandin, L., 1963: The objective analysis of meteorological fields, Leningrad, Gidrometeoizdat.

Graystone, P., 1962: The introduction of topographic and frictional effects in a baroclinic model, Quart, J. Roy. Meteor. Soc., 88, 256-270.

Harley, W., 1965: An operational method for quantitative precipitation forecasting, J. Appl. Meteor., 4, 305-319.

Hawkins, H. and S. Rosenthal, 1965: On the computation of stream-functions from the wind field, Mon. Wea. Rev., 93, 245-252.

Jarvis, E. and T. Agnew, 1970: A note on the computation of terrain and frictionally induced vertical velocities, J. Appl. Meteor., 9, 942-946.

McClain, P., 1960: Some effects of the Western Cordillera of North America on cyclonic activity, J. Meteor., 17, 104-115.

Murakami, T., 1956: The topographical effect upon the stationary upper flow pattern, Pap. Meteor. Geophys., 7, 69-89.

O'Neill, H., 1966: Vertical motion and precipitation computations, J. Appl. Meteor., 5, 595-605.

Petterssen, S., 1956: Weather Analysis and Forecasting, McGraw Hill Book Company, New York and London, Vol. 1, 428 pp.

Reinelt, E., 1970: On the role of orography in the precipitation regime of Alberta, The Albertan Geographer, 6, 45-58.

Reuter, H. and H. Pichler, 1964: On the orographic influences of the Alps, Tellus, 16, 40-42.

Sawyer, J., 1952: A study of the rainfall of two synoptic situations, Quart. J. Roy. Meteor. Soc., 78, 231-246.

_____, 1956: The physical and dynamical problems of orographic rain, Weather, 11, 375-381.

Smagorinsky, J. and G. Collins, 1955: On the numerical prediction of precipitation, Mon. Wea. Rev., 83, 53-68.

Sutton, O. G., 1949: The Science of Flight, Penguin Books, Harmondsworth Middlesex, 208 pp.

Tietjens, O., 1934: Fundamentals of hydro- and aero-mechanics, Translated by L. Rosenhead, McGraw Hill Book Company, Inc., New York and London, 270 pp.

Whitaker, S., 1968: Introduction to Fluid Mechanics, Prentice-Hall, Inc., Englewood Cliffs, N.J., 457 pp.

APPENDIX A

GRID POINT TOPOGRAPHIC PARAMETERS

PLUS

CORRESPONDING AVERAGE HEIGHT IN FEET

ROW	COLUMN	LATITUDE	LONGITUDE	AVERAGE HEIGHT(FEET)
20	14	74.30	134.46	0.
22	14	73.76	131.84	0.
24	14	73.19	129.40	0.
26	14	72.60	127.12	0.
28	14	71.97	125.00	60.
30	14	71.33	123.03	1500.
32	14	70.67	121.19	0.
34	14	69.99	119.47	0.
36	14	69.29	117.87	0.
38	14	68.59	116.38	500.
40	14	67.87	114.99	0.
42	14	67.14	113.69	1176.
44	14	66.40	112.47	1800.
46	14	65.65	111.33	1700.
48	14	64.90	110.26	1600.
50	14	64.14	109.25	1300.
52	14	63.38	108.30	1300.
54	14	62.61	107.41	1300.
56	14	61.84	106.57	1300.
58	14	61.07	105.77	1400.
60	14	60.29	105.02	1410.
62	14	59.51	104.30	1300.
64	14	58.73	103.63	1400.
66	14	57.95	102.99	1400.
68	14	57.17	102.38	1106.
70	14	56.39	101.80	1200.
72	14	55.61	101.25	1000.
74	14	54.83	100.73	1000.
76	14	54.05	100.22	838.
78	14	53.27	99.75	715.
80	14	52.49	99.29	850.
82	14	51.72	98.85	813.
84	14	50.94	98.43	813.
86	14	50.17	98.03	850.
88	14	49.40	97.65	780.

ROW	COLUMN	LATITUDE	LONGITUDE	AVERAGE HEIGHT(FEET)
20	15	73.56	136.31	0.
22	15	73.05	133.75	0.
24	15	72.50	131.34	0.
26	15	71.93	129.09	0.
28	15	71.33	126.97	0.
30	15	70.71	125.00	0.
32	15	70.07	123.15	0.
34	15	69.41	121.42	1600.
36	15	68.74	119.81	1800.
38	15	68.05	118.29	600.
40	15	67.35	116.87	836.
42	15	66.64	115.54	1800.
44	15	65.92	114.29	1500.
46	15	65.19	113.11	1400.
48	15	64.45	112.01	1400.
50	15	63.71	110.96	1400.
52	15	62.96	109.98	513.
54	15	62.20	109.05	1150.
56	15	61.44	108.18	1500.
58	15	60.68	107.35	1600.
60	15	59.92	106.57	1500.
62	15	59.15	105.82	1100.
64	15	58.38	105.11	1500.
66	15	57.61	104.44	1500.
68	15	56.84	103.81	1300.
70	15	56.07	103.20	1200.
72	15	55.30	102.62	1200.
74	15	54.52	102.07	977.
76	15	53.75	101.54	900.
78	15	52.98	101.04	875.
80	15	52.21	100.56	1000.
82	15	51.44	100.10	900.
84	15	50.68	99.65	1700.
86	15	49.91	99.23	1200.
88	15	49.15	98.82	1550.

ROW	COLUMN	LATITUDE	LONGITUDE	AVERAGE HEIGHT(FEET)
20	16	72.81	137.99	0.
22	16	72.32	135.49	0.
24	16	71.79	133.13	0.
26	16	71.24	130.91	0.
28	16	70.67	128.81	0.
30	16	70.07	126.85	0.
32	16	69.45	125.00	75.
34	16	68.81	123.26	1500.
36	16	68.16	121.63	1500.
38	16	67.49	120.10	1200.
40	16	66.81	118.66	1300.
42	16	66.11	117.30	1000.
44	16	65.41	116.03	1300.
46	16	64.70	114.82	1400.
48	16	63.98	113.69	1300.
50	16	63.25	112.62	1300.
52	16	62.51	111.61	513.
54	16	61.77	110.65	1100.
56	16	61.03	109.74	1300.
58	16	60.28	108.89	1700.
60	16	59.52	108.07	1300.
62	16	58.77	107.30	1400.
64	16	58.01	106.57	1500.
66	16	57.25	105.87	1700.
68	16	56.49	105.20	1700.
70	16	55.73	104.57	1400.
72	16	54.97	103.96	1300.
74	16	54.20	103.39	1150.
76	16	53.44	102.83	950.
78	16	52.68	102.31	1260.
80	16	51.92	101.80	1500.
82	16	51.15	101.32	1800.
84	16	50.39	100.85	1800.
86	16	49.64	100.41	1400.
88	16	48.88	99.98	2150.

ROW	COLUMN	LATITUDE	LONGITUDE	AVERAGE HEIGHT(FEET)
20	17	72.04	139.53	0.
22	17	71.57	137.09	0.
24	17	71.07	134.78	0.
26	17	70.54	132.59	0.
28	17	69.99	130.53	25.
30	17	69.41	128.58	200.
32	17	68.81	126.74	800.
34	17	68.20	125.00	1000.
36	17	67.56	123.36	1300.
38	17	66.91	121.82	900.
40	17	66.25	120.36	511.
42	17	65.57	118.99	1550.
44	17	64.88	117.69	1000.
46	17	64.19	116.47	950.
48	17	63.48	115.31	900.
50	17	62.77	114.22	800.
52	17	62.05	113.18	600.
54	17	61.32	112.20	700.
56	17	60.59	111.26	900.
58	17	59.85	110.38	1100.
60	17	59.11	109.54	700.
62	17	58.37	108.74	1500.
64	17	57.62	107.98	1750.
66	17	56.87	107.26	1550.
68	17	56.12	106.57	1400.
70	17	55.37	105.91	1300.
72	17	54.62	105.28	1650.
74	17	53.86	104.68	1650.
76	17	53.11	104.10	1200.
78	17	52.36	103.55	1900.
80	17	51.60	103.03	1700.
82	17	50.85	102.52	1730.
84	17	50.10	102.04	2000.
86	17	49.35	101.57	1750.
88	17	48.60	101.12	1500.

ROW	COLUMN	LATITUDE	LONGITUDE	AVERAGE HEIGHT(FEET)
20	18	71.26	140.95	0.
22	18	70.81	138.57	0.
24	18	70.33	136.31	0.
26	18	69.83	134.16	0.
28	18	69.29	132.12	50.
30	18	68.74	130.19	600.
32	18	68.16	128.37	500.
34	18	67.56	126.64	950.
36	18	66.95	125.00	1050.
38	18	66.31	123.45	511.
40	18	65.67	121.99	511.
42	18	65.01	120.60	650.
44	18	64.34	119.29	1200.
46	18	63.66	118.05	900.
48	18	62.97	116.87	925.
50	18	62.27	115.75	750.
52	18	61.57	114.70	513.
54	18	60.85	113.69	600.
56	18	60.14	112.74	725.
58	18	59.41	111.83	800.
60	18	58.68	110.96	700.
62	18	57.95	110.14	1200.
64	18	57.22	109.36	1600.
66	18	56.48	108.61	1400.
68	18	55.74	107.90	1300.
70	18	55.00	107.22	1600.
72	18	54.25	106.57	1800.
74	18	53.51	105.94	1700.
76	18	52.77	105.35	1600.
78	18	52.02	104.78	1800.
80	18	51.27	104.23	2350.
82	18	50.53	103.70	1940.
84	18	49.79	103.20	2300.
86	18	49.04	102.71	1900.
88	18	48.30	102.25	2200.

ROW	COLUMN	LATITUDE	LONGITUDE	AVERAGE HEIGHT(FEET)
20	19	70.48	142.24	0.
22	19	70.05	139.93	15.
24	19	69.59	137.72	22.
26	19	69.10	135.62	23.
28	19	68.59	133.62	275.
30	19	68.05	131.71	603.
32	19	67.49	129.90	732.
34	19	66.91	128.18	672.
36	19	66.31	126.55	872.
38	19	65.70	125.00	1038.
40	19	65.07	123.53	756.
42	19	64.43	122.14	918.
44	19	63.78	120.82	1080.
46	19	63.12	119.56	998.
48	19	62.44	118.37	948.
50	19	61.76	117.23	679.
52	19	61.07	116.16	607.
54	19	60.37	115.13	847.
56	19	59.66	114.16	1246.
58	19	58.95	113.23	926.
60	19	58.24	112.35	993.
62	19	57.52	111.50	1180.
64	19	56.80	110.70	1567.
66	19	56.07	109.93	1680.
68	19	55.34	109.20	1812.
70	19	54.61	108.50	1640.
72	19	53.87	107.82	1910.
74	19	53.14	107.18	1987.
76	19	52.40	106.57	1704.
78	19	51.67	105.97	1959.
80	19	50.93	105.41	1884.
82	19	50.20	104.86	2019.
84	19	49.46	104.34	2151.
86	19	48.72	103.84	2139.
88	19	47.99	103.36	2174.

ROW	COLUMN	LATITUDE	LONGITUDE	AVERAGE HEIGHT(FEET)
20	20	69.69	143.43	1297.
22	20	69.27	141.19	2077.
24	20	68.83	139.04	1440.
26	20	68.36	136.98	2184.
28	20	67.87	135.01	654.
30	20	67.35	133.13	369.
32	20	66.81	131.34	445.
34	20	66.25	129.64	355.
36	20	65.67	128.01	720.
38	20	65.07	126.47	925.
40	20	64.46	125.00	926.
42	20	63.84	123.60	927.
44	20	63.20	122.27	1066.
46	20	62.55	121.01	1150.
48	20	61.90	119.81	1149.
50	20	61.23	118.66	676.
52	20	60.55	117.57	1094.
54	20	59.87	116.53	1224.
56	20	59.18	115.54	2489.
58	20	58.48	114.59	1150.
60	20	57.78	113.69	1768.
62	20	57.07	112.83	1797.
64	20	56.36	112.01	1773.
66	20	55.64	111.22	2004.
68	20	54.92	110.47	2125.
70	20	54.20	109.74	1845.
72	20	53.48	109.05	2022.
74	20	52.76	108.39	1914.
76	20	52.03	107.76	1977.
78	20	51.30	107.15	2023.
80	20	50.58	106.57	2170.
82	20	49.85	106.00	2394.
84	20	49.12	105.46	2622.
86	20	48.39	104.94	2391.
88	20	47.66	104.44	2406.

ROW	COLUMN	LATITUDE	LONGITUDE	AVERAGE HEIGHT(FEET)
20	21	68.89	144.54	5097.
22	21	68.49	142.35	2902.
24	21	68.07	140.26	1167.
26	21	67.61	138.24	1397.
28	21	67.14	136.31	2130.
30	21	66.64	134.46	1090.
32	21	66.11	132.70	857.
34	21	65.57	131.01	2481.
36	21	65.01	129.40	3964.
38	21	64.43	127.86	4050.
40	21	63.84	126.40	2970.
42	21	63.23	125.00	2241.
44	21	62.61	123.67	2039.
46	21	61.98	122.40	1109.
48	21	61.34	121.19	978.
50	21	60.68	120.03	1394.
52	21	60.02	118.93	1754.
54	21	59.35	117.87	1332.
56	21	58.67	116.87	1338.
58	21	57.99	115.91	1191.
60	21	57.30	114.99	1727.
62	21	56.60	114.11	2123.
64	21	55.90	113.27	1960.
66	21	55.20	112.47	1983.
68	21	54.49	111.70	2006.
70	21	53.78	110.96	2026.
72	21	53.07	110.26	2100.
74	21	52.36	109.58	2150.
76	21	51.64	108.93	2193.
78	21	50.92	108.30	2196.
80	21	50.20	107.70	2574.
82	21	49.49	107.12	2650.
84	21	48.77	106.57	2871.
86	21	48.05	106.03	2227.
88	21	47.33	105.51	2574.

ROW	COLUMN	LATITUDE	LONGITUDE	AVERAGE HEIGHT(FEET)
20	22	68.08	145.56	2875.
22	22	67.70	143.43	1932.
24	22	67.30	141.39	1482.
26	22	66.86	139.42	2027.
28	22	66.40	137.53	1660.
30	22	65.92	135.71	2257.
32	22	65.41	133.97	3639.
34	22	64.88	132.31	4805.
36	22	64.34	130.71	5155.
38	22	63.78	129.18	5340.
40	22	63.20	127.73	5270.
42	22	62.61	126.33	5007.
44	22	62.01	125.00	3825.
46	22	61.39	123.73	2236.
48	22	60.76	122.51	1555.
50	22	60.12	121.35	1876.
52	22	59.47	120.24	1633.
54	22	58.82	119.17	1320.
56	22	58.15	118.16	1553.
58	22	57.48	117.18	1529.
60	22	56.81	116.25	2099.
62	22	56.12	115.36	2104.
64	22	55.44	114.51	2459.
66	22	54.74	113.69	2179.
68	22	54.05	112.91	2125.
70	22	53.35	112.15	2232.
72	22	52.65	111.43	2332.
74	22	51.94	110.74	2448.
76	22	51.24	110.07	2364.
78	22	50.53	109.43	2332.
80	22	49.82	108.81	3136.
82	22	49.11	108.22	2906.
84	22	48.40	107.65	2478.
86	22	47.69	107.10	2415.
88	22	46.98	106.57	2861.

ROW	COLUMN	LATITUDE	LONGITUDE	AVERAGE HEIGHT(FEET)
20	23	67.28	146.50	2095.
22	23	66.91	144.44	1116.
24	23	66.52	142.45	1241.
26	23	66.10	140.52	2372.
28	23	65.65	138.67	2612.
30	23	65.19	136.89	3432.
32	23	64.70	135.18	4192.
34	23	64.19	133.53	3482.
36	23	63.66	131.95	4510.
38	23	63.12	130.44	5020.
40	23	62.55	128.99	4837.
42	23	61.98	127.60	6050.
44	23	61.39	126.27	4247.
46	23	60.79	125.00	3670.
48	23	60.17	123.78	1537.
50	23	59.55	122.61	1731.
52	23	58.92	121.50	1714.
54	23	58.27	120.43	1678.
56	23	57.62	119.40	2729.
58	23	56.97	118.42	2599.
60	23	56.30	117.48	2091.
62	23	55.63	116.57	2181.
64	23	54.96	115.71	3161.
66	23	54.28	114.88	2456.
68	23	53.59	114.08	2481.
70	23	52.90	113.31	2577.
72	23	52.21	112.57	2670.
74	23	51.52	111.87	2594.
76	23	50.82	111.18	2428.
78	23	50.12	110.53	2565.
80	23	49.42	109.90	3224.
82	23	48.72	109.29	2834.
84	23	48.02	108.71	3158.
86	23	47.32	108.14	2899.
88	23	46.62	107.60	3154.

ROW	COLUMN	LATITUDE	LONGITUDE	AVERAGE HEIGHT(FEET)
20	24	66.47	147.38	1076.
22	24	66.11	145.38	997.
24	24	65.73	143.43	1566.
26	24	65.33	141.56	2165.
28	24	64.90	139.74	3137.
30	24	64.45	137.99	4317.
32	24	63.98	136.31	2956.
34	24	63.48	134.69	2179.
36	24	62.97	133.13	2990.
38	24	62.44	131.63	3925.
40	24	61.90	130.19	4452.
42	24	61.34	128.81	4145.
44	24	60.76	127.49	4260.
46	24	60.17	126.22	3455.
48	24	59.58	125.00	2777.
50	24	58.97	123.83	2505.
52	24	58.35	122.71	2031.
54	24	57.72	121.63	2446.
56	24	57.08	120.60	2541.
58	24	56.43	119.61	2479.
60	24	55.78	118.66	2056.
62	24	55.13	117.75	2232.
64	24	54.46	116.87	2821.
66	24	53.79	116.03	3079.
68	24	53.12	115.22	3024.
70	24	52.44	114.44	3185.
72	24	51.76	113.69	3092.
74	24	51.08	112.97	2917.
76	24	50.39	112.28	2706.
78	24	49.71	111.61	2976.
80	24	49.02	110.96	3362.
82	24	48.32	110.34	3005.
84	24	47.63	109.74	3467.
86	24	46.94	109.17	4207.
88	24	46.24	108.61	3687.

ROW	COLUMN	LATITUDE	LONGITUDE	AVERAGE HEIGHT(FEET)
20	25	65.65	148.20	1715.
22	25	65.31	146.25	2240.
24	25	64.95	144.36	2567.
26	25	64.56	142.53	2562.
28	25	64.14	140.75	2572.
30	25	63.71	139.04	2462.
32	25	63.25	137.38	2681.
34	25	62.77	135.78	2551.
36	25	62.27	134.25	4872.
38	25	61.76	132.77	4575.
40	25	61.23	131.34	4739.
42	25	60.68	129.97	3532.
44	25	60.12	128.65	3117.
46	25	59.55	127.39	2757.
48	25	58.97	126.17	4432.
50	25	58.37	125.00	4705.
52	25	57.76	123.88	4545.
54	25	57.15	122.80	3925.
56	25	56.52	121.76	2577.
58	25	55.89	120.76	2554.
60	25	55.25	119.81	2706.
62	25	54.61	118.88	3251.
64	25	53.96	118.00	4162.
66	25	53.30	117.15	4635.
68	25	52.64	116.33	5337.
70	25	51.97	115.54	4992.
72	25	51.30	114.78	4742.
74	25	50.63	114.05	4128.
76	25	49.95	113.34	3427.
78	25	49.28	112.66	3806.
80	25	48.60	112.01	3553.
82	25	47.91	111.37	3311.
84	25	47.23	110.76	4657.
86	25	46.55	110.17	5606.
88	25	45.86	109.60	5476.

ROW	COLUMN	LATITUDE	LONGITUDE	AVERAGE HEIGHT(FEET)
20	26	64.84	148.96	640.
22	26	64.51	147.07	1005.
24	26	64.16	145.22	2020.
26	26	63.78	143.43	2802.
28	26	63.38	141.70	2362.
30	26	62.96	140.02	2530.
32	26	62.51	138.39	3330.
34	26	62.05	136.82	3642.
36	26	61.57	135.30	3292.
38	26	61.07	133.84	4495.
40	26	60.55	132.43	3734.
42	26	60.02	131.07	3547.
44	26	59.47	129.76	3730.
46	26	58.92	128.50	4405.
48	26	58.35	127.29	3872.
50	26	57.76	126.12	4357.
52	26	57.17	125.00	4962.
54	26	56.57	123.92	3572.
56	26	55.96	122.88	4370.
58	26	55.34	121.88	3630.
60	26	54.71	120.91	4210.
62	26	54.08	119.99	5550.
64	26	53.44	119.09	6540.
66	26	52.79	118.23	6582.
68	26	52.14	117.41	6910.
70	26	51.49	116.61	7077.
72	26	50.83	115.84	5842.
74	26	50.17	115.10	6827.
76	26	49.50	114.38	5252.
78	26	48.84	113.69	5555.
80	26	48.16	113.02	5387.
82	26	47.49	112.38	4676.
84	26	46.82	111.76	5174.
86	26	46.14	111.16	5581.
88	26	45.47	110.58	6376.

ROW	COLUMN	LATITUDE	LONGITUDE	AVERAGE HEIGHT(FEET)
20	27	64.02	149.68	1887.
22	27	63.71	147.83	3172.
24	27	63.36	146.04	4315.
26	27	63.00	144.29	3090.
28	27	62.61	142.59	3264.
30	27	62.20	140.95	3086.
32	27	61.77	139.35	4137.
34	27	61.32	137.80	4207.
36	27	60.85	136.31	3432.
38	27	60.37	134.87	3370.
40	27	59.87	133.47	3335.
42	27	59.35	132.12	3137.
44	27	58.82	130.83	4045.
46	27	58.27	129.57	4430.
48	27	57.72	128.37	4842.
50	27	57.15	127.20	5022.
52	27	56.57	126.08	5382.
54	27	55.98	125.00	4717.
56	27	55.38	123.96	3850.
58	27	54.78	122.95	3427.
60	27	54.16	121.99	2915.
62	27	53.54	121.05	5312.
64	27	52.91	120.16	6215.
66	27	52.28	119.29	5282.
68	27	51.64	118.45	4165.
70	27	51.00	117.65	4997.
72	27	50.35	116.87	5260.
74	27	49.70	116.12	4935.
76	27	49.04	115.39	5150.
78	27	48.38	114.70	4444.
80	27	47.72	114.02	4377.
82	27	47.06	113.37	5156.
84	27	46.39	112.74	5517.
86	27	45.73	112.12	6165.
88	27	45.06	111.53	6812.

ROW	COLUMN	LATITUDE	LONGITUDE	AVERAGE HEIGHT(FEET)
20	28	63.20	150.35	5050.
22	28	62.90	148.55	3030.
24	28	62.57	146.80	2749.
26	28	62.22	145.10	2169.
28	28	61.84	143.43	4940.
30	28	61.44	141.82	4957.
32	28	61.03	140.26	7267.
34	28	60.59	138.74	2882.
36	28	60.14	137.26	4037.
38	28	59.66	135.84	3430.
40	28	59.18	134.46	4605.
42	28	58.67	133.13	3880.
44	28	58.15	131.84	3641.
46	28	57.62	130.60	4131.
48	28	57.08	129.40	5277.
50	28	56.52	128.24	4340.
52	28	55.96	127.12	5585.
54	28	55.38	126.04	3985.
56	28	54.80	125.00	3042.
58	28	54.20	123.99	2700.
60	28	53.60	123.03	2970.
62	28	52.99	122.09	3130.
64	28	52.38	121.19	3190.
66	28	51.75	120.31	3970.
68	28	51.13	119.47	4075.
70	28	50.49	118.66	4685.
72	28	49.86	117.87	4690.
74	28	49.22	117.12	4430.
76	28	48.57	116.38	3145.
78	28	47.92	115.68	3461.
80	28	47.27	114.99	4206.
82	28	46.62	114.33	5490.
84	28	45.96	113.69	6572.
86	28	45.30	113.07	7132.
88	28	44.65	112.47	6781.

ROW	COLUMN	LATITUDE	LONGITUDE	AVERAGE HEIGHT(FEET)
20	29	62.38	150.97	2172.
22	29	62.09	149.23	2572.
24	29	61.77	147.52	4599.
26	29	61.43	145.85	3584.
28	29	61.07	144.23	3682.
30	29	60.68	142.65	2910.
32	29	60.28	141.11	5016.
34	29	59.85	139.62	1544.
36	29	59.41	138.17	3104.
38	29	58.95	136.77	2776.
40	29	58.48	135.41	2677.
42	29	57.99	134.09	1084.
44	29	57.48	132.82	2895.
46	29	56.97	131.58	2522.
48	29	56.43	130.39	4550.
50	29	55.89	129.24	2642.
52	29	55.34	128.12	3025.
54	29	54.78	127.05	3452.
56	29	54.20	126.01	3202.
58	29	53.62	125.00	3312.
60	29	53.03	124.03	3917.
62	29	52.43	123.09	4032.
64	29	51.83	122.18	3585.
66	29	51.22	121.31	3600.
68	29	50.60	120.46	3515.
70	29	49.98	119.64	3700.
72	29	49.35	118.85	3221.
74	29	48.72	118.09	2876.
76	29	48.09	117.35	2531.
78	29	47.45	116.63	2824.
80	29	46.81	115.94	2957.
82	29	46.17	115.27	5425.
84	29	45.52	114.62	6756.
86	29	44.87	114.00	6387.
88	29	44.22	113.39	6576.

ROW	COLUMN	LATITUDE	LONGITUDE	AVERAGE HEIGHT(FEET)
20	30	61.57	151.57	1732.
22	30	61.28	149.86	780.
24	30	60.97	148.20	1845.
26	30	60.64	146.57	1117.
28	30	60.29	144.98	607.
30	30	59.92	143.43	495.
32	30	59.52	141.93	64.
34	30	59.11	140.46	19.
36	30	58.68	139.04	19.
38	30	58.24	137.65	559.
40	30	57.78	136.31	237.
42	30	57.30	135.01	380.
44	30	56.81	133.75	435.
46	30	56.30	132.52	765.
48	30	55.78	131.34	1270.
50	30	55.25	130.19	1515.
52	30	54.71	129.09	3305.
54	30	54.16	128.01	3792.
56	30	53.60	126.97	4082.
58	30	53.03	125.97	3352.
60	30	52.45	125.00	4245.
62	30	51.87	124.06	4198.
64	30	51.27	123.15	5758.
66	30	50.68	122.27	5855.
68	30	50.07	121.42	3909.
70	30	49.46	120.60	3086.
72	30	48.84	119.81	4092.
74	30	48.22	119.04	2500.
76	30	47.60	118.29	2066.
78	30	46.97	117.57	2209.
80	30	46.34	116.87	2767.
82	30	45.71	116.19	5087.
84	30	45.07	115.54	7096.
86	30	44.43	114.90	8335.
88	30	43.79	114.29	7596.

ROW	COLUMN	LATITUDE	LONGITUDE	AVERAGE HEIGHT(FEET)
20	31	60.75	152.12	1430.
22	31	60.47	150.46	650.
24	31	60.17	148.84	3025.
26	31	59.85	147.25	210.
28	31	59.51	145.70	0.
30	31	59.15	144.18	0.
32	31	58.77	142.70	0.
34	31	58.37	141.26	0.
36	31	57.95	139.86	0.
38	31	57.52	138.50	0.
40	31	57.07	137.17	0.
42	31	56.60	135.89	120.
44	31	56.12	134.64	180.
46	31	55.63	133.43	150.
48	31	55.13	132.25	540.
50	31	54.61	131.12	67.
52	31	54.08	130.01	1042.
54	31	53.54	128.95	772.
56	31	52.99	127.91	2362.
58	31	52.43	126.91	4102.
60	31	51.87	125.94	6105.
62	31	51.29	125.00	4661.
64	31	50.71	124.09	5276.
66	31	50.12	123.21	5075.
68	31	49.53	122.36	2804.
70	31	48.93	121.53	3299.
72	31	48.32	120.73	4540.
74	31	47.71	119.96	2417.
76	31	47.10	119.21	1351.
78	31	46.48	118.48	1471.
80	31	45.86	117.78	3874.
82	31	45.24	117.09	4766.
84	31	44.61	116.43	4057.
86	31	43.98	115.79	5742.
88	31	43.35	115.17	5390.

ROW	COLUMN	LATITUDE	LONGITUDE	AVERAGE HEIGHT(FEET)
20	32	59.93	152.65	765.
22	32	59.66	151.03	440.
24	32	59.37	149.44	225.
26	32	59.06	147.89	0.
28	32	58.73	146.37	0.
30	32	58.38	144.89	0.
32	32	58.01	143.43	0.
34	32	57.62	142.02	0.
36	32	57.22	140.64	0.
38	32	56.80	139.30	0.
40	32	56.36	137.99	0.
42	32	55.90	136.73	0.
44	32	55.44	135.49	0.
46	32	54.96	134.29	0.
48	32	54.46	133.13	105.
50	32	53.96	132.00	215.
52	32	53.44	130.91	15.
54	32	52.91	129.84	90.
56	32	52.38	128.81	187.
58	32	51.83	127.82	1010.
60	32	51.27	126.85	3047.
62	32	50.71	125.91	2125.
64	32	50.14	125.00	1267.
66	32	49.56	124.12	697.
68	32	48.98	123.26	465.
70	32	48.39	122.44	665.
72	32	47.80	121.63	2340.
74	32	47.20	120.86	2525.
76	32	46.59	120.10	2383.
78	32	45.99	119.37	1250.
80	32	45.37	118.66	3871.
82	32	44.76	117.97	5226.
84	32	44.14	117.30	3197.
86	32	43.52	116.66	3297.
88	32	42.90	116.03	3829.

ROW	COLUMN	LATITUDE	LONGITUDE	AVERAGE HEIGHT(FEET)
20	33	59.11	153.14	150.
22	33	58.86	151.57	112.
24	33	58.57	150.02	0.
26	33	58.27	148.50	0.
28	33	57.95	147.01	0.
30	33	57.61	145.56	0.
32	33	57.25	144.13	0.
34	33	56.87	142.74	0.
36	33	56.48	141.39	0.
38	33	56.07	140.07	0.
40	33	55.64	138.78	0.
42	33	55.20	137.53	0.
44	33	54.74	136.31	0.
46	33	54.28	135.12	0.
48	33	53.79	133.97	75.
50	33	53.30	132.85	105.
52	33	52.79	131.77	30.
54	33	52.28	130.71	0.
56	33	51.75	129.69	0.
58	33	51.22	128.69	0.
60	33	50.68	127.73	632.
62	33	50.12	126.79	1837.
64	33	49.56	125.88	1547.
66	33	49.00	125.00	577.
68	33	48.43	124.14	540.
70	33	47.85	123.32	2547.
72	33	47.26	122.51	911.
74	33	46.67	121.73	2757.
76	33	46.08	120.97	2868.
78	33	45.48	120.24	1974.
80	33	44.88	119.52	3900.
82	33	44.27	118.83	5430.
84	33	43.66	118.16	4337.
86	33	43.05	117.50	4505.
88	33	42.44	116.87	5953.

ROW	COLUMN	LATITUDE	LONGITUDE	AVERAGE HEIGHT(FEET)
20	34	58.30	153.61	630.
22	34	58.05	152.07	180.
24	34	57.78	150.56	0.
26	34	57.48	149.08	0.
28	34	57.17	147.62	0.
30	34	56.84	146.19	0.
32	34	56.49	144.80	0.
34	34	56.12	143.43	0.
36	34	55.74	142.10	0.
38	34	55.34	140.80	0.
40	34	54.92	139.53	0.
42	34	54.49	138.30	0.
44	34	54.05	137.09	0.
46	34	53.59	135.92	0.
48	34	53.12	134.78	0.
50	34	52.64	133.67	0.
52	34	52.14	132.59	0.
54	34	51.64	131.55	0.
56	34	51.13	130.53	0.
58	34	50.60	129.54	0.
60	34	50.07	128.58	0.
62	34	49.53	127.64	0.
64	34	48.98	126.74	0.
66	34	48.43	125.86	0.
68	34	47.86	125.00	52.
70	34	47.30	124.17	517.
72	34	46.72	123.36	2457.
74	34	46.14	122.58	1577.
76	34	45.56	121.82	2879.
78	34	44.97	121.08	2111.
80	34	44.38	120.36	4417.
82	34	43.78	119.67	4792.
84	34	43.18	118.99	4671.
86	34	42.58	118.33	4986.
88	34	41.97	117.69	5085.

ROW	COLUMN	LATITUDE	LONGITUDE	AVERAGE HEIGHT(FEET)
20	35	57.48	154.05	1250.
22	35	57.24	152.55	405.
24	35	56.98	151.08	0.
26	35	56.69	149.62	0.
28	35	56.39	148.20	0.
30	35	56.07	146.80	0.
32	35	55.73	145.43	0.
34	35	55.37	144.09	0.
36	35	55.00	142.78	0.
38	35	54.61	141.50	0.
40	35	54.20	140.26	0.
42	35	53.78	139.04	0.
44	35	53.35	137.85	0.
46	35	52.90	136.69	0.
48	35	52.44	135.56	0.
50	35	51.97	134.46	0.
52	35	51.49	133.39	0.
54	35	51.00	132.35	0.
56	35	50.49	131.34	0.
58	35	49.98	130.36	0.
60	35	49.46	129.40	0.
62	35	48.93	128.47	0.
64	35	48.39	127.56	0.
66	35	47.85	126.68	0.
68	35	47.30	125.83	0.
70	35	46.74	125.00	0.
72	35	46.17	124.19	124.
74	35	45.60	123.41	889.
76	35	45.03	122.65	898.
78	35	44.45	121.91	3882.
80	35	43.87	121.19	4691.
82	35	43.28	120.49	4577.
84	35	42.69	119.81	4722.
86	35	42.10	119.14	5839.
88	35	41.50	118.50	4687.

ROW	COLUMN	LATITUDE	LONGITUDE	AVERAGE HEIGHT(FEET)
20	36	56.67	154.48	45.
22	36	56.43	153.01	0.
24	36	56.18	151.57	0.
26	36	55.90	150.14	0.
28	36	55.61	148.75	0.
30	36	55.30	147.38	0.
32	36	54.97	146.04	0.
34	36	54.62	144.72	0.
36	36	54.25	143.43	0.
38	36	53.87	142.18	0.
40	36	53.48	140.95	0.
42	36	53.07	139.74	0.
44	36	52.65	138.57	0.
46	36	52.21	137.43	0.
48	36	51.76	136.31	0.
50	36	51.30	135.22	0.
52	36	50.83	134.16	0.
54	36	50.35	133.13	0.
56	36	49.86	132.12	0.
58	36	49.35	131.15	0.
60	36	48.84	130.19	0.
62	36	48.32	129.27	0.
64	36	47.80	128.37	0.
66	36	47.26	127.49	0.
68	36	46.72	126.64	0.
70	36	46.17	125.81	0.
72	36	45.62	125.00	0.
74	36	45.06	124.22	90.
76	36	44.50	123.45	601.
78	36	43.93	122.71	1899.
80	36	43.35	121.99	4881.
82	36	42.78	121.28	5300.
84	36	42.20	120.60	5256.
86	36	41.61	119.94	6057.
88	36	41.02	119.29	5147.

ROW	COLUMN	LATITUDE	LONGITUDE	AVERAGE HEIGHT(FEET)
20	37	55.86	154.88	0.
22	37	55.63	153.44	0.
24	37	55.38	152.03	0.
26	37	55.11	150.64	0.
28	37	54.83	149.27	0.
30	37	54.52	147.93	0.
32	37	54.20	146.61	0.
34	37	53.86	145.32	0.
36	37	53.51	144.06	0.
38	37	53.14	142.82	0.
40	37	52.76	141.61	0.
42	37	52.36	140.42	0.
44	37	51.94	139.26	0.
46	37	51.52	138.13	0.
48	37	51.08	137.03	0.
50	37	50.63	135.95	0.
52	37	50.17	134.90	0.
54	37	49.70	133.88	0.
56	37	49.22	132.88	0.
58	37	48.72	131.91	0.
60	37	48.22	130.96	0.
62	37	47.71	130.04	0.
64	37	47.20	129.14	0.
66	37	46.67	128.27	0.
68	37	46.14	127.42	0.
70	37	45.60	126.59	0.
72	37	45.06	125.78	0.
74	37	44.51	125.00	0.
76	37	43.96	124.24	232.
78	37	43.40	123.49	1175.
80	37	42.83	122.77	3285.
82	37	42.27	122.06	4852.
84	37	41.69	121.38	4469.
86	37	41.12	120.71	5171.
88	37	40.54	120.06	5214.

ROW	COLUMN	LATITUDE	LONGITUDE	AVERAGE HEIGHT(FEET)
20	38	55.05	155.26	0.
22	38	54.83	153.86	0.
24	38	54.59	152.47	0.
26	38	54.33	151.11	0.
28	38	54.05	149.78	0.
30	38	53.75	148.46	0.
32	38	53.44	147.17	0.
34	38	53.11	145.90	0.
36	38	52.77	144.65	0.
38	38	52.40	143.43	0.
40	38	52.03	142.24	0.
42	38	51.64	141.07	0.
44	38	51.24	139.93	0.
46	38	50.82	138.81	0.
48	38	50.39	137.72	0.
50	38	49.95	136.66	0.
52	38	49.50	135.62	0.
54	38	49.04	134.61	0.
56	38	48.57	133.62	0.
58	38	48.09	132.65	0.
60	38	47.60	131.71	0.
62	38	47.10	130.79	0.
64	38	46.59	129.90	0.
66	38	46.08	129.03	0.
68	38	45.56	128.18	0.
70	38	45.03	127.35	0.
72	38	44.50	126.55	0.
74	38	43.96	125.76	0.
76	38	43.41	125.00	7.
78	38	42.86	124.26	947.
80	38	42.31	123.53	1987.
82	38	41.75	122.83	4410.
84	38	41.19	122.14	3520.
86	38	40.62	121.47	4395.
88	38	40.05	120.82	4331.

ROW	COLUMN	LATITUDE	LONGITUDE	AVERAGE HEIGHT(FEET)
20	39	54.24	155.62	0.
22	39	54.03	154.25	0.
24	39	53.79	152.90	0.
26	39	53.54	151.57	0.
28	39	53.27	150.25	0.
30	39	52.98	148.96	0.
32	39	52.68	147.69	0.
34	39	52.36	146.45	0.
36	39	52.02	145.22	0.
38	39	51.67	144.03	0.
40	39	51.30	142.85	0.
42	39	50.92	141.70	0.
44	39	50.53	140.57	0.
46	39	50.12	139.47	0.
48	39	49.71	138.39	0.
50	39	49.28	137.34	0.
52	39	48.84	136.31	0.
54	39	48.38	135.30	0.
56	39	47.92	134.32	0.
58	39	47.45	133.37	0.
60	39	46.97	132.43	0.
62	39	46.48	131.52	0.
64	39	45.99	130.63	0.
66	39	45.48	129.76	0.
68	39	44.97	128.92	0.
70	39	44.45	128.09	0.
72	39	43.93	127.29	0.
74	39	43.40	126.51	0.
76	39	42.86	125.74	0.
78	39	42.32	125.00	120.
80	39	41.78	124.27	585.
82	39	41.23	123.57	2657.
84	39	40.67	122.88	3000.
86	39	40.11	122.21	1257.
88	39	39.55	121.55	1647.

ROW	COLUMN	LATITUDE	LONGITUDE	AVERAGE HEIGHT(FEET)
20	40	53.44	155.96	0.
22	40	53.23	154.62	0.
24	40	53.00	153.30	0.
26	40	52.76	152.00	0.
28	40	52.49	150.71	0.
30	40	52.21	149.44	0.
32	40	51.92	148.20	0.
34	40	51.60	146.97	0.
36	40	51.27	145.77	0.
38	40	50.93	144.59	0.
40	40	50.58	143.43	0.
42	40	50.20	142.30	0.
44	40	49.82	141.19	0.
46	40	49.42	140.10	0.
48	40	49.02	139.04	0.
50	40	48.60	137.99	0.
52	40	48.16	136.98	0.
54	40	47.72	135.98	0.
56	40	47.27	135.01	0.
58	40	46.81	134.06	0.
60	40	46.34	133.13	0.
62	40	45.86	132.22	0.
64	40	45.37	131.34	0.
66	40	44.88	130.48	0.
68	40	44.38	129.64	0.
70	40	43.87	128.81	0.
72	40	43.35	128.01	0.
74	40	42.83	127.23	0.
76	40	42.31	126.47	0.
78	40	41.78	125.73	0.
80	40	41.24	125.00	0.
82	40	40.70	124.29	435.
84	40	40.15	123.60	1622.
86	40	39.60	122.93	3556.
88	40	39.05	122.27	782.

ROW	COLUMN	LATITUDE	LONGITUDE	AVERAGE HEIGHT(FEET)
20	41	52.64	156.29	0.
22	41	52.43	154.98	0.
24	41	52.21	153.69	0.
26	41	51.97	152.41	0.
28	41	51.72	151.15	0.
30	41	51.44	149.90	0.
32	41	51.15	148.68	0.
34	41	50.85	147.48	0.
36	41	50.53	146.30	0.
38	41	50.20	145.14	0.
40	41	49.85	144.00	0.
42	41	49.49	142.88	0.
44	41	49.11	141.78	0.
46	41	48.72	140.71	0.
48	41	48.32	139.66	0.
50	41	47.91	138.63	0.
52	41	47.49	137.62	0.
54	41	47.06	136.63	0.
56	41	46.62	135.67	0.
58	41	46.17	134.73	0.
60	41	45.71	133.81	0.
62	41	45.24	132.91	0.
64	41	44.76	132.03	0.
66	41	44.27	131.17	0.
68	41	43.78	130.33	0.
70	41	43.28	129.51	0.
72	41	42.78	128.72	0.
74	41	42.27	127.94	0.
76	41	41.75	127.17	0.
78	41	41.23	126.43	0.
80	41	40.70	125.71	0.
82	41	40.17	125.00	0.
84	41	39.63	124.31	60.
86	41	39.09	123.64	872.
88	41	38.55	122.98	872.

ROW	COLUMN	LATITUDE	LONGITUDE	AVERAGE HEIGHT(FEET)
20	42	51.84	156.61	0.
22	42	51.64	155.32	0.
24	42	51.42	154.05	0.
26	42	51.19	152.80	0.
28	42	50.94	151.57	0.
30	42	50.68	150.35	0.
32	42	50.39	149.15	0.
34	42	50.10	147.96	0.
36	42	49.79	146.80	0.
38	42	49.46	145.66	0.
40	42	49.12	144.54	0.
42	42	48.77	143.43	0.
44	42	48.40	142.35	0.
46	42	48.02	141.29	0.
48	42	47.63	140.26	0.
50	42	47.23	139.24	0.
52	42	46.82	138.24	0.
54	42	46.39	137.26	0.
56	42	45.96	136.31	0.
58	42	45.52	135.38	0.
60	42	45.07	134.46	0.
62	42	44.61	133.57	0.
64	42	44.14	132.70	0.
66	42	43.66	131.84	0.
68	42	43.18	131.01	0.
70	42	42.69	130.19	0.
72	42	42.20	129.40	0.
74	42	41.69	128.62	0.
76	42	41.19	127.86	0.
78	42	40.67	127.12	0.
80	42	40.15	126.40	0.
82	42	39.63	125.69	0.
84	42	39.10	125.00	0.
86	42	38.57	124.33	0.
88	42	38.04	123.67	7.

APPENDIX B

I. Derivation of radius r of a latitude circle and of the map factor σ on a polar stereographic map projection true at latitude ϕ.

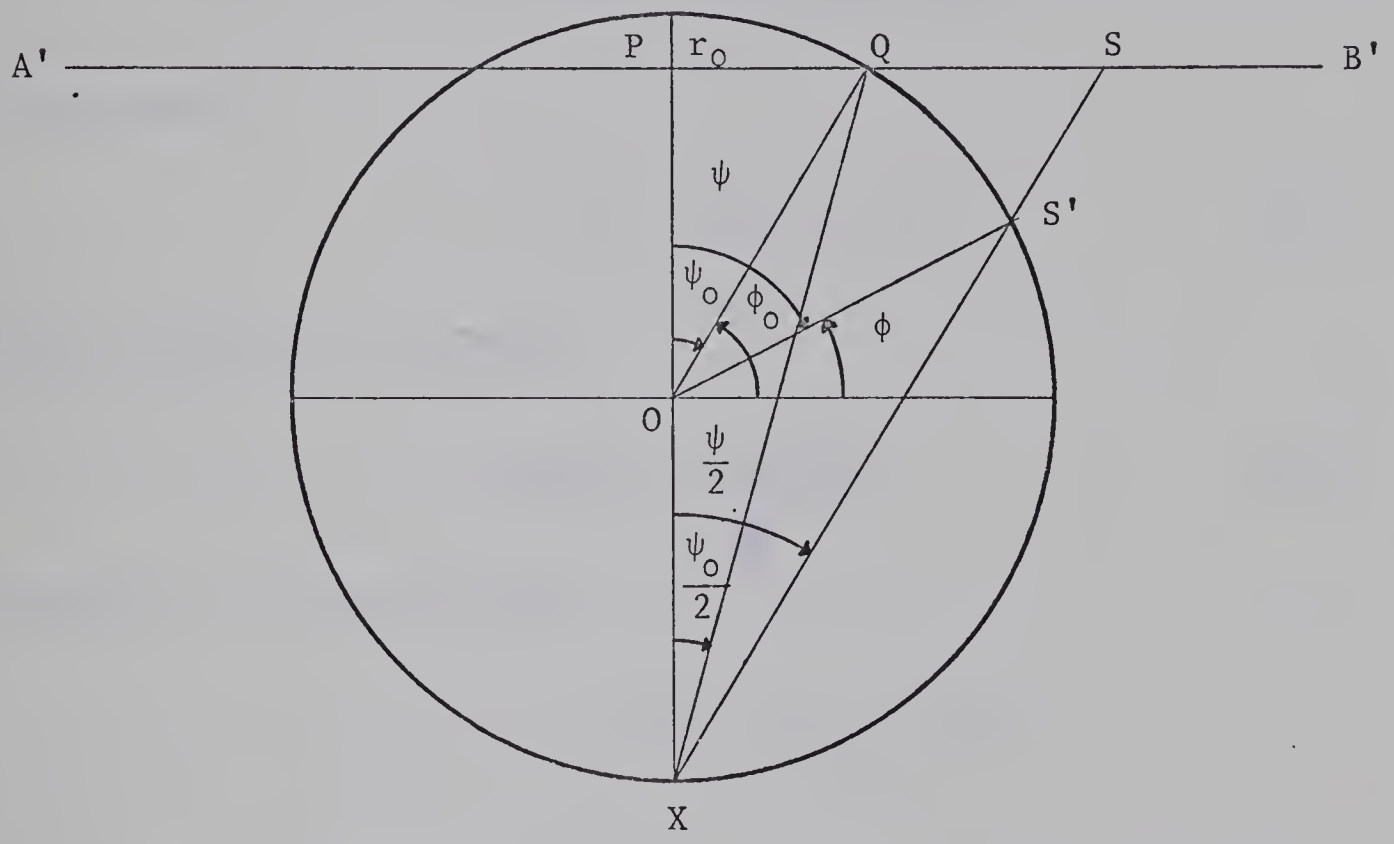

FIGURE (B-1) Cross-section of the earth with its center at O. A'B' is a plane cutting the earth at latitude ϕ_o. ϕ is any latitude, x the south pole, and ψ, ψ_o, colatitudes of ϕ and ϕ_o respectively. XS'S is the projection of S' in plane A'B'.

Let

$$PS = r$$

$$PQ = r_o$$

and

$$QO = a = \text{radius of the spherical earth.}$$

From Figure (B-1) it can be seen that

$$PO = a \cos \psi_o .$$

Therefore,

$$PX = a + a \cos \psi_o .$$

From the triangle PXS

$$\tan \frac{\psi}{2} = \frac{PS}{PX} = \frac{r}{a(1 + \cos \psi_o)} .$$

Consequently,

$$r = a(1 + \cos \psi_o) \tan \frac{\psi}{2} . \qquad \text{(B-1)}$$

From trigonometric relations

$$\tan \frac{\psi}{2} = \frac{\sin \psi}{1 + \cos \psi} . \qquad \text{(B-2)}$$

Therefore, by equation (B-1)

$$r = \frac{a(1 + \cos \psi_o) \sin \psi}{1 + \cos \psi} ,$$

and in terms of latitude

$$r = \frac{a\ (1 + \sin \phi_o) \cos \phi}{(1 + \sin \phi)} . \qquad \text{(B-3)}$$

The map factor σ is defined as

$$\sigma \equiv \frac{\text{Image Distance}}{\text{Earth Distance}} . \qquad \text{(B-4)}$$

The length of a latitude circle L on the map is equal to $2\pi r$. Its length on the earth is $2\pi a \cos \phi$. Equation (B-4) becomes

$$\sigma = \frac{2\pi r}{2\pi a \cos \phi} , \qquad \text{(B-5)}$$

and from equation (B-3)

$$\sigma = \frac{1 + \sin \phi_o}{1 + \sin \phi} \quad . \qquad \text{(B-6)}$$

II. Calculation of Grid Point Location

Let the grid length be d cm and the radius of a latitude circle on the map be r cm. From equation (B-1)

$$r = a(1 + \sin \phi_o) \tan \frac{\psi}{2} \times m \ , \qquad \text{(B-7)}$$

where m is the scale of the map which is used because r × 1/m is equivalent to the distance on earth. (m is a ratio, e.g., 1 : 10^7). Equation (B-7) can be rewritten as

$$\psi = 2 \tan^{-1} \frac{1/m \times r}{a(1 + \sin \phi_o)} \quad . \qquad \text{(B-8)}$$

Since ψ is a colatitude

$$\phi = 90° - \psi, \text{ with } \psi \text{ expressed in degrees.}$$

Therefore, the latitude of any grid point can be obtained by equation (B-8) provided r is known. For example consider the following grid:

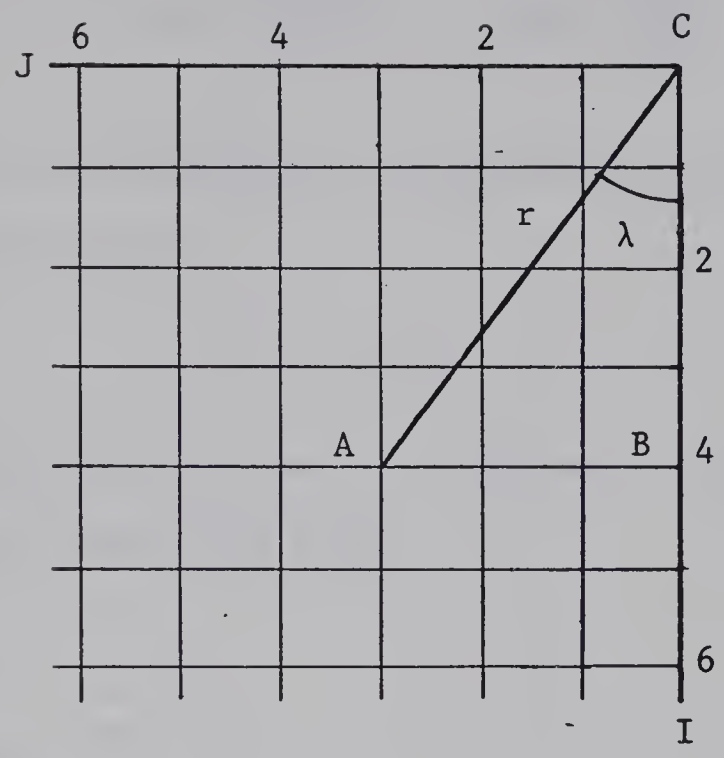

FIGURE (B-2) Section of a grid with grid length d. A is an arbitrary grid point and C is located at the North Pole. λ is the deviation of AC = r from a reference line BC of the grid.

From triangle ABC, since C is the North Pole and AC the radius r of a latitude circle on the map,

$$AC = r = \left[(BC)^2 + (AB)^2 \right]^{1/2}$$

whence,

$$r = \left[(4d)^2 + (3d)^2 \right]^{1/2} .$$

Since d is constant and known, the latitude of grid point A can be calculated.

Since the angles between longitude lines are conserved on this type of map projection, the longitude of A can also be computed. All that is required to be known is the longitude of a reference line of the grid. If BC is such a line in Figure (B-2) and if λ is the

deviation of AC from BC, then

$$\lambda = \tan^{-1}\left(\frac{AB}{BC}\right) = \tan^{-1}\left(\frac{3d}{4d}\right) . \qquad \text{(B-9)}$$

If the longitude of BC is 80°W (as for the grid in this study), then the real longitude of A is

$$80° + \lambda .$$

The geographic coordinates of any grid point can thus be found from equations (B-8) and (B-9).

APPENDIX C

INDEX OF STATIONS

COMPUTER NO.	INDEX NO.	NAME	LAT.	LONG.	ELEVATION (Meters)	CLASSIFICATION*
1	072	Mould Bay, N.W.T.	76 14N	119 20W	15	RS
2	026	Barrow, Alas.	71 18N	156 47W	4	RS
3	051	Sachs Harbour, N.W.T.	71 59N	125 17W	84	RS
4	086	Barter Island, Alas.	70 08N	143 38W	15	RS
5	968	Aklavik, N.W.T.	68 14N	135 00W	10	RS
6	938	Coppermine, N.W.T.	67 50N	115 07W	00	RS
7	222	Galena, Alas.	64 40N	157 00W	49	P
8	261	Fairbanks, Alas.	64 49N	147 52W	138	RS
9	043	Norman Wells, N.W.T.	65 17N	126 48W	64	RS
10	926	Baker Lake, N.W.T.	64 18N	96 00W	00	RS
11	231	McGrath, Alas.	62 58N	155 37W	103	RS
12	219	Bethel, Alas.	60 47N	161 43W	46	RS
13	273	Anchorage, Alas.	61 10N	150 01W	40	RS
14	200	Gonzales Heights, B.C.	48 25N	123 19W	69	P
15	964	Whitehorse, Y.T.	60 43N	135 04W	816	RS
16	953	Watson Lake, Y.T.	60 07N	128 49W	685	P
17	934	Fort Smith, N.W.T.	60 01N	111 58W	203	RS
18	326	King Salmon, Alas.	58 41N	156 39W	15	RS
19	936	Yellowknife, N.W.T.	62 28N	114 27W	208	P
20	361	Yakutat, Alas.	59 31N	139 40W	9	RS
21	316	Cold Bay, Alas.	55 12N	162 43W	31	RS
22	350	Kodiak, Alas.	57 45N	152 31W	34	RS
23	1111	Pacific Ocean	58 00N	145 00W	00	DE
24	381	Juneau, Alas.	58 22N	135 55W	7	P

* RS - RADIOSONDE STATION

P - PIBAL STATION

DE - DATA ESTIMATES

COMPUTER NO.	INDEX NO.	NAME	LAT.	LONG.	ELEVATION (Meters)	CLASSIFICATION
25	958	Dease Lake, B.C.	58 25N	133 00W	816	DE
26	945	Fort Nelson, B.C.	58 50N	122 35W	375	RS
27	913	Churchill, Man.	58 45N	94 04W	35	RS
28	939	Beatton River, B.C.	57 23N	121 23W	839	DE
29	932	Fort McMurray, Alta.	56 39N	111 13W	371	P
30	2221	Pacific Ocean	55 00N	150 00W	00	DE
31	2222	Pacific Ocean	55 00N	145 00W	00	DE
32	2223	Pacific Ocean	55 00N	140 00W	00	DE
33	398	Annette, Alas.	55 02N	131 34W	34	RS
34	940	Grande Prairie, Alta.	55 11N	118 53W	668	P
35	069	Wagner, Alta.	55 21N	114 59W	583	P
36	120	Cold Lake, Alta.	54 25N	110 17W	544	P
37	896	Prince George, B.C.	53 53N	122 41W	676	RS
38	879	Edmonton, Alta.	53 34N	113 31W	676	RS
39	869	Prince Albert, Sask.	53 13N	105 41W	431	P
40	867	The Pas, Man.	53 58N	101 06W	272	RS
41	848	Trout Lake, Ont.	53 50N	89 52W	219	RS
42	888	Jasper, Alta.	52 53N	118 04W	1016	DE
43	928	Rocky Mountain House, Alta.	52 23N	114 55W	1015	DE
44	878	Red Deer, Alta.	52 11N	113 54W	904	DE
45	873	Coronation, Alta.	52 06N	111 27W	798	DE
46	111	Dog Creek, B.C.	51 38N	122 15W	1027	DE
47	877	Calgary, Alta.	51 06N	114 01W	1079	P
48	855	Dauphin, Man.	51 06N	100 03W	305	P
49	109	Port Hardy, B.C.	50 41N	127 22W	23	RS
50	870	Swift Current, Sask.	50 17N	107 41W	816	DE
51	863	Regina, Sask.	50 26N	104 40W	574	P
52	3331	Pacific Ocean	50 00N	145 00W	00	DE
53	3332	Pacific Ocean	52 00N	140 00W	00	DE
54	3333	Pacific Ocean	50 00N	135 00W	00	DE
55	860	Rivers, Man.	50 01N	100 19W	475	P
56	852	Winnipeg, Man.	49 54N	97 14W	240	P
57	842	Sioux Lookout, Ont.	50 07N	91 54W	374	P

COMPUTER NO.	INDEX NO.	NAME	LAT.	LONG.	ELEVATION (Meters)	CLASSIFICATION
58	893	Comox, B.C.	49 43N	124 54W	23	P
59	880	Kimberley, B.C.	49 44N	115 47W	930	DE
60	874	Lethbridge, Alta.	49 38N	112 48W	920	P
61	4441	Pacific Ocean	48 00N	139 00W	00	DE
62	4442	Pacific Ocean	49 00N	130 00W	00	DE
63	798	Tatoosh Island, Wash.	48 23N	124 44W	25	RS
64	777	Havre City County, Mont.	48 34N	109 40W	792	P
65	747	International Falls, Minn.	48 34N	93 23W	361	RS
66	793	Seattle, Wash.	47 27N	122 15W	137	RS
67	785	Spokane, Wash.	47 37N	117 31W	721	RS
68	775	Great Falls, Mont.	47 29N	111 21W	1115	RS
69	768	Glasgow, Mont.	48 13N	106 37W	700	RS
70	767	Williston, N.Dak.	48 11N	103 38W	581	P
71	783	Lewiston, Idaho	46 23N	117 01W	438	P
72	677	Billings, Mont.	45 48N	108 32W	1088	P
73	764	Bismark, N.Dak.	46 46N	100 45W	506	RS
74	753	Fargo, N.Dak.	46 54N	96 48W	274	P
75	745	Duluth, Minn.	46 47N	92 11W	432	P
76	4443	Pacific Ocean	45 00N	140 00W	00	DE
77	4444	Pacific Ocean	45 00N	135 00W	00	DE
78	4445	Pacific Ocean	45 00N	130 00W	00	DE
79	694	Salem, Oreg.	44 55N	123 01W	61	RS
80	773	Missoula, Mont.	46 55N	114 05W	972	P
81	666	Sheridan, Wyo.	44 46N	106 58W	1209	P
82	655	St. Cloud, Minn.	45 35N	94 11W	318	RS
83	681	Boise, Idaho	43 34N	116 13W	871	RS
84	597	Medford, Oreg.	42 22N	122 52W	405	RS
85	583	Winnemucca, Nev.	40 54N	117 48W	1322	RS
86	576	Lander, Wyo.	42 49N	108 44W	1694	RS
87	662	Rapid City, S.Dak.	44 03N	103 04W	966	RS
88	654	Huron, S.Dak.	44 23N	98 13W	393	P

COMPUTER NO.	INDEX NO.	NAME	LAT.	LONG.	ELEVATION (Meters)	CLASSIFICATION
89	572	Salt Lake City, Utah	40 46N	111 58W	1288	RS
90	5551	Pacific Ocean	40 00N	135 00W	00	DE
91	5552	Pacific Ocean	40 00N	130 00W	00	DE
92	486	Ely, Nev.	39 17N	114 51W	1909	DE
93	493	Oakland, Calif.	47 44N	122 12W	3	RS
94	6661	Pacific Ocean	35 00N	135 00W	00	DE
95	6662	Pacific Ocean	35 00N	130 00W	00	DE
96	6663	Pacific Ocean	35 00N	125 00W	00	DE
97	394	Santa Maria, Calif.	34 54N	120 27W	73	RS
98	295	Los Angeles, Calif.	33 56N	118 24W	32	DE
99	290	San Diego, Calif.	32 44N	117 10W	9	DE
100	386	Las Vegas, Nev.	36 05N	115 10W	664	RS
101	476	Grand Junction, Colo.	39 07N	108 32W	1475	RS
102	469	Denver, Colo.	29 46N	104 53W	1625	RS
103	464	Pueblo, Colo.	38 17N	104 31W	1439	P
104	562	North Platte, Nebr.	41 08N	100 41W	849	RS
105	557	Sioux City, Iowa	42 24N	96 23W	336	P
106	553	Omaha, Nebr.	41 22N	96 01W	406	RS
107	546	Des Moines, Iowa	41 32N	93 39W	294	P
108	643	La Crosse, Wis.	43 52N	91 15W	220	P
109	645	Green Bay, Wis.	44 29N	88 08W	214	RS
110	734	Sault Ste. Marie, Mich.	46 28N	84 22W	221	RS
111	831	Kapuskasing, Ont.	49 25N	82 28W	229	P
112	133	Kotzebue, Alas.	66 52N	162 38W	5	RS
113	200	Nome, Alas.	64 30N	165 26W	7	RS
114	8800	Pacific Ocean	54 00N	135 00W	00	DE
115	8801	Mountains, B.C.	57 00N	125 00W	838	DE
116	8882	Mountains, B.C.	54 00N	129 30W	762	DE